FIRST-PRINCIPLES DESIGN MAPS FOR PREDICTING ANOMALOUS DUCTILITY IN B2 MATERIALS

BY

RUOSHI SUN

THESIS

Submitted in partial fulfillment of the requirements
for the degree of Bachelor of Science in Materials Science and Engineering
in the College of Engineering of the
University of Illinois at Urbana-Champaign, 2008

Urbana, Illinois

Abstract

Recently, a new class of B2 intermetallic compounds, e.g., YAg and YCu, were experimentally shown to have significant ductility comparable to face-centered cubic (fcc) Al, in contrast to other B2 materials like CuZn or NiAl. As of yet, there has been no explanation for the enhanced ductility in this class of materials. In order to provide understanding and a means to predict for such behavior, we derive, using mesoscale dislocation mechanics, criteria of $\langle 111 \rangle$ slip versus $\langle 001 \rangle$ slip, as well as the relative stability of antiphase boundaries (APB) and stacking faults (SF), together giving the necessary condition for ductility. Combined with the sufficient condition, which requires APB bistability on $\{1\bar{1}0\}$ and $\{11\bar{2}\}$ planes, stability maps are constructed using dimensionless ratios of the calculated lattice constants, elastic constants, $\frac{a}{2}\langle 111 \rangle \{1\bar{1}0\}$ and $\frac{a}{2}\langle 111 \rangle \{11\bar{2}\}$ APB energies, and $\frac{a}{2}\langle 001 \rangle \{1\bar{1}0\}$ SF energies. To obtain required input to the stability maps, we have performed first-principles density-functional theory (DFT) calculations on three types of B2 materials: the Y-based B2 compounds (YAg, YCu, YIn, YRh, and YMg), the classic B2 alloys (NiAl, FeAl, AuCd, AuZn, CuZn, and AgMg), and the CsCl-type ionic compounds (CsCl, CsI, TlBr, and TlCl). In all the B2 materials, only YAg and YRh satisfy both necessary and sufficient conditions for enhanced ductility, while, like classic B2 alloys and ionic compounds, the YIn and YMg systems are predicted to be brittle, where the latter has been experimentally confirmed. This general combined dislocation mechanics and DFT approach provides predictive maps for use in alloy design and understanding of anomalous ductility in B2 systems.

To my parents

Acknowledgements

I would like to thank Professor Duane Johnson for his guidance and help throughout my summer REU project in 2007 and my thesis project. Being constantly cheerful and encouraging, he has always brought a lively atmosphere to our office and has helped us through dead-ends. I remember he warned me many times of a common pitfall in computational materials science: getting the numbers "correct" (i.e., agreeing with experiment) is not necessarily physically correct. Not only did he teach me techniques in performing first-principles calculations, but also, more importantly, he demonstrated the ability to formulate the right questions and capture the right physics. He made me realize that being a professor involved much more than conducting research.

We acknowledge Dr. Karl Gschneidner, Jr. of Ames Laboratory for helpful comments on the brittleness of YMg, and Prof. James Morris of Oak Ridge National Laboratory for discussion on the competing stability of B33 and B27 phases. Funding and computational support were provided by the National Science Foundation (grants DMR-0312448, for the 2007 summer REU project, and DMR-07-05089) and the Department of Energy (grants DEFG02-03ER46026 and DEFG02-91ER45439 at the Frederick Seitz Materials Research Laboratory). We also acknowledge additional computational support from a faculty INTEL grant.

I thank Professor Jian-Min Zuo for being my undergraduate academic advisor and letting me conduct research for him since I was a freshman. He got my foot in the door when my first serious project began in the summer of 2006. I thank him for his hospitality in inviting me to have Thanksgiving dinner with his family.

I thank Professor John Abelson and Dr. Raju Perecherla for organizing the REU program; Professors Johnson, Zuo, and Dallas Trinkle for their support and invaluable advice regarding graduate school applications, and their patience in writing the recommendation letters.

I thank my officemates, Fakhruddin Bohra, Dr. Ayten Celik-Aktas, Dr. Hao Chen, Dr. Weijie Huang, Li Ji, Dr. Seongwon Kim, Dr. Taekyung Kim, Dr. Boquan Li, Dr. Hyuk Park, Dr. Kazuhisa Sato, Amish Shah, Shankar Sivaramakrishnan, Dr. Jing Tao, and Jiong Zhang of Professor Zuo's group, and Dr. Aftab Alam, Dominic Biava, Dr. Brent Kraczek, Dr. Jian-Bo Liu, Teck Tan, and Dr. Lin-Lin Wang of Professor Johnson's group, for their availability and advice, especially Dr. Huang and Dr. Liu for being my REU mentors.

I thank numerous professors of the math department: Professors Joseph Miles and John D'Angelo for recommending honors courses; Professors Marius Junge, Jeremy Tyson, D'Angelo, Zhong-Jin Ruan, and especially Sergei Ivanov for their rigorous teaching of the honors sequence; Professors Junge and Ilya Kapovich for helpful comments on typesetting math equations in LaTeX; Professor Randy McCarthy for encouraging me to apply for a double degree in math; Professor Bruce Reznick for his lively teaching of complex analysis, and, fortunately, I understood the course material more than his jokes (showing that math really transcends cultural boundaries); and Professors Richard Laugesen and Stephanie Alexander for granting me the wish of taking their courses for honors credit. I thank Professor D'Angelo for being my unofficial advisor in math and for playing weiqi/go with me. I am amazed by his skills.

I thank my friends, especially Sihan, for showing me the beauty and love that can only take place outside the ivory tower, and for bearing with me when I had to be in the tower. I thank Tony for bringing me to ICCF.

Last but not least, I thank my parents for raising me up, and for letting me understand the meaning of "home sweet home," when home shrunk to a spot on the other side of the world.

Table of Contents

List of Tables

List of Figures

List of Abbreviations

APB	Antiphase boundary
bcc	Body-centered cubic
DFT	Density-functional theory
fcc	Face-centered cubic
GGA	Generalized gradient approximation
PAW	Projected augmented wave
RM	Rare earth/transition metal
SF	Stacking fault
SISF	Superintrinsic stacking fault
VASP	Vienna Ab-initio Simulation Package

Chapter 1

Introduction

In 2003, Gschneidner *et al.* [1] discovered a family of ductile intermetallic compounds with the body-centered cubic (bcc) based B2 (CsCl) crystal structure, see Figure 1.1. These compounds are composed of rare earth/transition metals (RM), including YAg, YCu, YIn, YRh, DyCu, CeAg, ErAg, ErAu, ErCu, ErIr, HoCu, and NdAg, among others. The ductility of YAg is comparable to face-centered cubic (fcc) Al, much higher than that of the classic B2 NiAl and CuZn alloys, for example, whereas the ductility of YCu is about half that of YAg. The engineering stress-strain curves for YCu and YAg are shown in Figure 1.2 [1]. It is known that line compounds are usually brittle [2]; hence, the reason for high ductility in RM compounds remains an open question. Moreover, some RM compounds, such as $(Tb_{0.88}Dy_{0.12})Zn$ [3] and YMg [4], are brittle, which raises the question: Why are they different?

Much work has been done in determining experimentally, as well as predicting theoretically, the slip systems of the classic B2 alloys. As discussed in the extensive review articles by Yamaguchi and Umakoshi [5] and Baker [6], $\langle 111 \rangle$ and $\langle 001 \rangle$ are the two main slip directions for dislocation motion observed in B2 materials (Fig. 1.3). Rachinger and Cottrell [7] attempted to predict the slip direction via ordering energy and the extent of metallic bonding versus ionic bonding. However, as pointed out by Ball and Smallman [8], NiAl and AuZn would be predicted to exhibit $\langle 111 \rangle$ slip instead of the observed $\langle 001 \rangle$ slip. Using anisotropic elasticity theory and Bragg-Williams approximation of antiphase boundary (APB) energies, Potter successfully predicted the operative slip systems in CsBr, NiAl, CuZn, AuZn, and AuCd [9]. Yet no previous theoretical treatments have attempted to predict the ductility

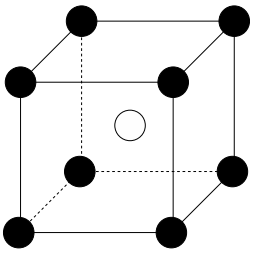

Figure 1.1: Unit cell of the B2 structure. Filled and open circles represent different atomic species. It resembles the body-centered cubic (bcc) structure, in which case only one element is present.

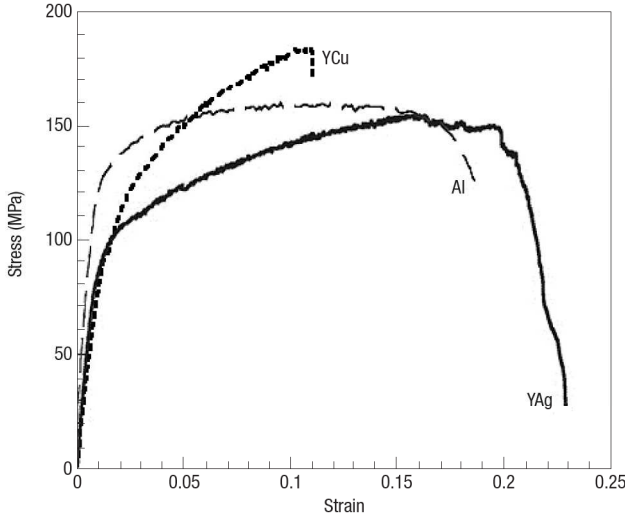

Figure 1.2: Tensile stress-strain curves of YAg, YCu, compared with fcc Al. (Reprinted by permission from Macmillan Publishers Ltd: Nature Materials 2:587–591 © 2003.)

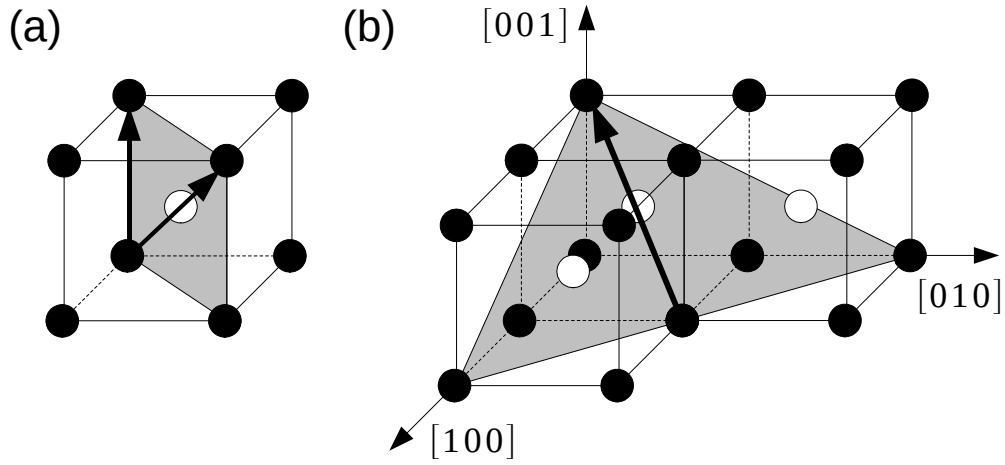

Figure 1.3: Slip directions in B2 systems. (a) [001] and [111] slip directions in the $(1\bar{1}0)$ plane. (b) $[\bar{1}\bar{1}1]$ slip direction in the (112) plane.

of B2 materials, since all the known classic B2 alloys and ionic compounds are brittle. For example, polycrystalline NiAl has only a 2% elongation upon fracture [2]. Baker concluded that limited ductility is associated with $\langle 001 \rangle$ slip, and brittleness with $\langle 111 \rangle$ slip [6]. While off-stoichiometric B2 alloys exhibit improved ductility, yield strength is sacrificed, which is not useful for practical purposes [2].

In sharp contrast to the classic B2 alloys, the new class of RM intermetallic compounds have an exact stoichiometry. Also, they are nearly elastically isotropic [1], with Zener anisotropy ratios close to 1, defined by

$$A = \frac{2c_{44}}{c_{11} - c_{12}}, \tag{1.1}$$

where the c_{ij}'s are the standard cubic elastic constants. There have been many recent efforts following the discovery of these RM compounds, including both experimental [3, 10, 11] and theoretical [12, 13, 14] investigations. Morris and Ye [14] have hypothesized that the enhanced ductility in the Y-based compounds is due to the competing structural stability of B33 and B27 phases, which can be obtained by introducing a periodic array of $\frac{a}{2}\langle 001 \rangle \{1\bar{1}0\}$ stacking faults (SF) to the B2 lattice. However, as mentioned earlier, not all RM intermetallic compounds are ductile. This brings further complications to the classification of the slip modes in B2 materials and the prediction of their ductility.

To address the atypical ductility possessed by most of the RM compounds, as well as the unresolved issue of predicting $\langle 111 \rangle$ versus $\langle 001 \rangle$ slip directions, we attempt to provide a quantitative explanation using mesoscale dislocation mechanics with direct input from first-principles density-functional theory (DFT) calculations. In a recent study of the $L1_2$ pseudo-binary alloy $(Ni_{1-c}Fe_c)_3Ge$, Liu, Johnson, and Smirnov [15] successfully predicted yield-stress anomaly by considering the *necessary* (stability of APB versus superintrinsic stacking fault (SISF)) and *sufficient* (stability of APB(111) versus APB(100)) conditions for cross-slip of screw dislocation segments, and calculating the APB and SISF energies

from first-principles. The necessary and sufficient criteria were worked out, respectively, by Paidar, Pope, and Yamaguchi [16] and Saada and Veyssiere [17]. The resulting stability map, however, is applicable to any $L1_2$ material. Here, we adopt a similar approach to study competing slip modes in B2 systems. As in the $L1_2$ case, design maps can be constructed based on stability criteria derived in the B2 crystal structure.

Three types of B2 materials are investigated in this study: (1) the Y-based B2 compounds (YAg, YCu, YIn, YRh, and YMg); (2) the classic B2 alloys (NiAl, FeAl, AuCd, AuZn, CuZn, and AgMg); and (3) the CsCl-type ionic compounds (CsCl, CsI, TlBr, and TlCl). Off-stoichiometric disorder will not be introduced. In the following chapters, we shall first present the conditions for different slip modes, especially comparing $\langle 001 \rangle$ versus $\langle 111 \rangle$ slip, the relative stability of APB and SF formation, and APB bistability on $\{1\bar{1}0\}$ and $\{11\bar{2}\}$ planes. These will give the *necessary* and *sufficient* conditions for enhanced ductility. Next, we will define and derive quantities for computation, including APB and SF energies, lattice parameters and elastic constants, as well as various quantities used in plotting the stability maps. As we will see, these quantities are dimensionless ratios of defect energies and/or elastic constants. Therefore, any systematic error in the first-principles calculations will be ameliorated. Details of calculation methods will be presented for completeness and reproducibility, specifying the unit cells, translation vectors, k-point meshes, and relaxation. Finally, calculated properties will be compared with available experimental values and other calculation results. The stability maps will be analyzed and the atypical ductility of RM compounds will be explained.

In short, only YAg and YRh satisfy both the necessary and sufficient conditions, while the YIn and YMg systems, the classic B2 alloys, and the CsCl-type ionic compounds do not. We predict YAg and YRh to be highly ductile, YCu to be half as ductile, and the remainder to be brittle, in agreement with reported findings, see Figure 1.2 and Refs. [1, 4].

Chapter 2

Background

To achieve the goal of this project, we pose the following questions:

1. Can we provide predictive maps that separate various B2 materials into their favorable slip modes?

2. How well do the predicted slip modes compare with the experimentally observed slip systems?

3. Can these results explain the atypical ductility observed in the RM compounds?

In this chapter, we shall address the first question by considering several energy-based criteria for competing slip modes in B2 systems. The last two questions will be discussed based on the predictive maps that involve competing stability of APBs and SFs, and effects of elastic anisotropy.

2.1 B2 Stability Maps for Competing Slip Modes

2.1.1 Necessary condition: $\langle 111 \rangle \{1\bar{1}0\}$ versus $\langle 001 \rangle \{1\bar{1}0\}$

Multiple slip can occur via formation of $\langle 111 \rangle$ APBs because the APBs exist on two families of planes, namely, $\{1\bar{1}0\}$ and $\{11\bar{2}\}$. It is necessary, then, that the formation of $\langle 111 \rangle$ APBs has to be more energetically favorable than the formation of $\langle 001 \rangle$ SFs. To predict $\langle 111 \rangle$ versus $\langle 001 \rangle$ slip, Rachinger and Cottrell [7] gave a simple criterion: If $w_{\mathrm{APB}} \gg a$, then $\langle 111 \rangle$ slip is favorable; else if $w_{\mathrm{APB}} \approx a$, then $\langle 001 \rangle$ is favorable. We derive a more quantitative

criterion as follows, in light of Paidar, Pope, and Yamaguchi's work in $L1_2$ systems [16]. (See Appendix A for the derivation in $L1_2$ systems.)

Saada and Veysseiere [18] investigated the condition for cross-slip of a $\langle 111 \rangle$ screw superdislocation on $\{1\bar{1}0\}$ and $\{11\bar{2}\}$ planes, where the latter is the Kear-Wilsdorf configuration of the B2 crystal structure. The possible dissociation mechanisms for a $\langle 111 \rangle$ screw superdislocation are:

$$a\langle 111\rangle \rightarrow a\langle 110\rangle + a\langle 001\rangle \rightarrow a\langle 100\rangle + a\langle 010\rangle + a\langle 001\rangle \tag{2.1}$$

$$a\langle 001\rangle \rightarrow \frac{a}{2}\langle 001\rangle + \mathrm{SF} + \frac{a}{2}\langle 001\rangle \tag{2.2}$$

$$a\langle 111\rangle \rightarrow \frac{a}{2}\langle 111\rangle + \mathrm{APB} + \frac{a}{2}\langle 111\rangle. \tag{2.3}$$

For simplicity, the APBs and SFs shall be denoted by their defect planes; i.e., $\frac{a}{2}\langle 111\rangle\{1\bar{1}0\}$ and $\frac{a}{2}\langle 111\rangle\{11\bar{2}\}$ APBs will be referred to as APB$\{1\bar{1}0\}$ and APB$\{11\bar{2}\}$, respectively, and SF $\frac{a}{2}\langle 001\rangle\{1\bar{1}0\}$ will be denoted as SF$\{1\bar{1}0\}$. We shall compare these three processes based on their energetics. Recall that the self energies of a screw and an edge dislocation are [19]

$$E_s = \frac{Gb_s^2}{4\pi}\ln\frac{r}{r_0} \tag{2.4}$$

$$E_e = \frac{Gb_e^2}{4\pi(1-\nu)}\ln\frac{r}{r_0}, \tag{2.5}$$

where $G = c_{44}$ is the shear modulus, b_s and b_e are the Burgers vectors of the screw and edge dislocations, respectively, r_0 is the radius of the dislocation core, and r is the cutoff radius of dislocation interaction. We note that r is finite because its strain field is canceled by the strain field of other dislocations [20]. The pure screw and edge interaction energies are [19]

$$E_{ss} = \frac{Gb_s^2}{2\pi}\ln\frac{r}{w} \tag{2.6}$$

$$E_{ee} = \frac{Gb_e^2}{2\pi(1-\nu)}\ln\frac{r}{w}, \tag{2.7}$$

where w is the separation distance between APBs or SFs.

In Eq. (2.1), the $\langle 111 \rangle$ screw dislocation dissociates into perfect dislocations along the cube edges (Fig. 2.1), hence there are no APBs or SFs. The dissociation does not result in any change in the total energy. Thus, with $\mathbf{b}_{1s} = a\langle 111 \rangle$ and $b_{1s}^2 = 3a^2$, the total energy of the screw dislocation is

$$E_1 = \frac{Gb_{1s}^2}{4\pi} \ln \frac{r}{r_0} = \frac{3Ga^2}{4\pi} \ln \frac{r}{r_0}. \tag{2.8}$$

Equation (2.2) shows that the $a\langle 001 \rangle$ dislocation can further dissociate into $\frac{a}{2}\langle 001 \rangle$ partial dislocations, creating an intrinsic stacking fault. The screw and edge components of the partial dislocation can be found by projecting $\frac{a}{2}\langle 001 \rangle$ onto $a\langle 111 \rangle$:

$$\frac{a}{2}\langle 001 \rangle = \underbrace{\frac{a}{6}\langle 111 \rangle}_{\mathbf{b}_{2s}} + \underbrace{\frac{a}{6}\langle \bar{1}\bar{1}2 \rangle}_{\mathbf{b}_{2e}}. \tag{2.9}$$

Thus, with $b_{2s}^2 = a^2/12$ and $b_{2e}^2 = a^2/6$, the self energies are

$$E_{2s} = \frac{Ga^2}{48\pi} \ln \frac{r}{r_0} \tag{2.10}$$

$$E_{2e} = \frac{Ga^2}{24\pi(1-\nu)} \ln \frac{r}{r_0}; \tag{2.11}$$

the interaction energies are

$$E_{2ss} = \frac{Ga^2}{24\pi} \ln \frac{r}{w_{\mathrm{SF}}} \tag{2.12}$$

$$E_{2ee} = \frac{Ga^2}{12\pi(1-\nu)} \ln \frac{r}{w_{\mathrm{SF}}}. \tag{2.13}$$

The total energy associated with SF formation is then

$$E_2 = \frac{Ga^2}{24\pi} \left(\ln \frac{r}{r_0} + \ln \frac{r}{w_{\mathrm{SF}}} \right) + \frac{Ga^2}{12\pi(1-\nu)} \left(\ln \frac{r}{r_0} + \ln \frac{r}{w_{\mathrm{SF}}} \right) + \gamma_{\mathrm{SF}} w_{\mathrm{SF}}. \tag{2.14}$$

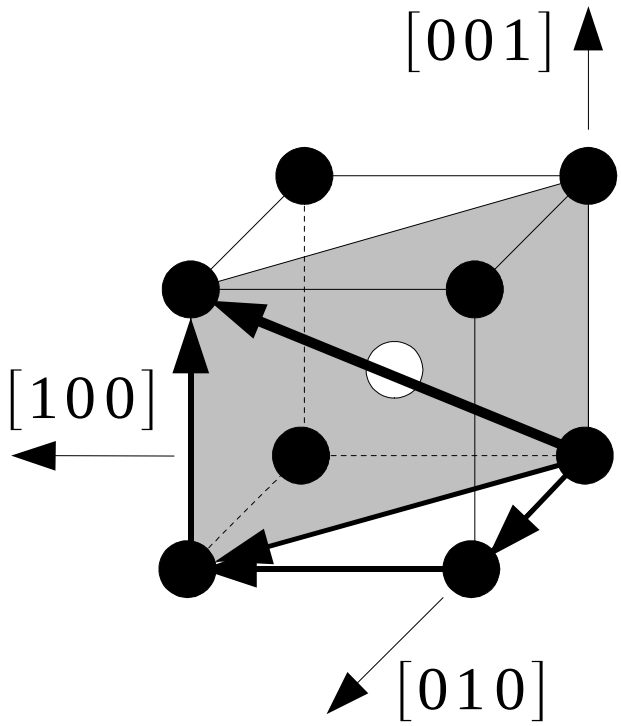

Figure 2.1: Perfect dissociation of a $\langle 111 \rangle$ superdislocation in B2 systems (Eq. (2.1)). Perfect $\langle 110 \rangle$ and $\langle 001 \rangle$ dislocations are created in the first step. $\langle 110 \rangle$ can further dissociate into $\langle 100 \rangle$ and $\langle 010 \rangle$.

The separation width $w_{\rm SF}$ can be found by setting $\frac{\partial E_2}{\partial w_{\rm SF}} = 0$, yielding

$$w_{\rm SF} = \frac{3-\nu}{1-\nu}\frac{Ga^2}{24\pi\gamma_{\rm SF}}. \tag{2.15}$$

Then Eq. (2.14) becomes

$$E_2 = \frac{3-\nu}{1-\nu}\frac{Ga^2}{24\pi}\left(\ln\frac{r}{r_0} + \ln\frac{r}{w_{\rm SF}} + 1\right). \tag{2.16}$$

Lastly, the $\langle 111\rangle$ screw dislocation can dissociate into two $\frac{1}{2}\langle 111\rangle$ partials bounding an APB, as shown in Eq. (2.3). The partials are purely screw, with Burgers vector $\mathbf{b}_{3s} = \frac{a}{2}\langle 111\rangle$ and $b_{3s}^2 = 3a^2/4$. Given the separation width $w_{\rm APB}$ of the partials, with planar defect energy $\gamma_{\rm APB}$, the total energy is

$$E_3 = 2E_{3s} + E_{3ss} + \gamma_{\rm APB} w_{\rm APB}. \tag{2.17}$$

We minimize Eq. (2.17) with respect to $w_{\rm APB}$ to get

$$w_{\rm APB} = \frac{Gb_{3s}^2}{2\pi\gamma_{\rm APB}} = \frac{3Ga^2}{8\pi\gamma_{\rm APB}}. \tag{2.18}$$

Then Eq. (2.17) becomes

$$E_3 = \frac{3Ga^2}{8\pi}\left(\ln\frac{r}{r_0} + \ln\frac{r}{w_{\rm APB}} + 1\right). \tag{2.19}$$

We can now compare perfect dissociation into $\langle 001\rangle$ slip systems (Eq. (2.1)) versus dissociation into screw partials with associated APB formation (Eq. (2.3)). Based purely on energy grounds, in order for $\langle 001\rangle\{1\bar{1}0\}$ slip to be more favorable than APB$\{1\bar{1}0\}$ formation, we require E_1 in Eq. (2.8) to be less than E_3 in Eq. (2.19):

$$\begin{aligned} \frac{3Ga^2}{4\pi}\ln\frac{r}{r_0} &< \frac{3Ga^2}{8\pi}\left(\ln\frac{r}{r_0} + \ln\frac{r}{w_{\rm APB}} + 1\right) \\ \ln\frac{w_{\rm APB}}{r_0} &< 1. \end{aligned} \tag{2.20}$$

The dislocation core can be written as $r_0 = ka$ for some constant k. Then, by Eq. (2.20), the condition for $\langle 001 \rangle$ slip is

$$\frac{w_{\mathrm{APB}}^{1\bar{1}0}}{a} < ke, \tag{2.21}$$

which can be rewritten in terms of the planar defect energy as

$$\frac{\gamma_{\mathrm{APB}}^{1\bar{1}0}}{Ga} > \frac{3}{8\pi ke}. \tag{2.22}$$

The core of the dislocation can be simulated using semi-empirical and first-principles calculations, from which the radius of the core, and hence k, can be obtained for each B2 material. In general, r_0 is roughly between b and $5b$ [21], so k is between $\sqrt{3}/2$ and $5\sqrt{3}/2$ in our case. Eshelby [22] estimated analytically r_0 to be about $1.5b$ for screw dislocations, which, according to Read [23], is an underestimation. A simulation study by Xu and Moriarty shows that $2b$, where $\mathbf{b} = \frac{a}{2}\langle 111 \rangle$, is a good approximation for r_0 in bcc Mo. We expect the core radius to be somewhat larger in B2 systems than in bcc metals, since $\mathbf{b}$ represents a partial dislocation in B2, instead of a perfect dislocation in bcc. Thus, we shall simply take r_0 to be between $2.5b$ ($k \approx 2.17$) and $5b$ ($k \approx 4.33$) for all B2 materials. Then ke in Eq. (2.21) is between 5.9 and 11.8, which justifies the criterion imposed by Rachinger and Cottrell, but provides a quantitative measure for comparison of many systems.

Next we compare SF formation (Eq. (2.2)) with APB formation (Eq. (2.3)). Notice that we should multiply E_2 by 3 for a fair comparison, since each $\langle 111 \rangle$ dislocation dissociates into three families of $\langle 001 \rangle$ dislocations, where each of them can create SFs independently. In order for APBs to be more energetically favorable than SFs, we need E_3 in Eq. (2.19) to be less than $3E_2$ in Eq. (2.16) :

$$\begin{aligned} \frac{3Ga^2}{8\pi}\left(\ln\frac{r}{r_0} + \frac{r}{w_{\mathrm{APB}}} + 1\right) &< 3 \times \frac{3-\nu}{1-\nu}\frac{Ga^2}{24\pi}\left(\ln\frac{r}{r_0} + \ln\frac{r}{w_{\mathrm{SF}}} + 1\right) \\ 3\ln\frac{r}{w_{\mathrm{APB}}} - \frac{2\nu}{1-\nu}\left(1 + \ln\frac{r}{r_0}\right) &< \frac{3-\nu}{1-\nu}\ln\frac{r}{w_{\mathrm{SF}}}. \end{aligned} \tag{2.23}$$

Writing $r_0 = ka$, we get

$$\begin{aligned} 3\left(\ln\frac{a}{w_{\mathrm{APB}}} + \ln\frac{r}{a}\right) - \frac{2\nu}{1-\nu}\left(1 + \ln\frac{r}{ka}\right) &< \frac{3-\nu}{1-\nu}\left(\ln\frac{a}{w_{\mathrm{SF}}} + \ln\frac{r}{a}\right) \\ 3\ln\frac{8\pi\gamma_{\mathrm{APB}}}{3Ga} - \frac{2\nu}{1-\nu}\left(1 + 2\ln\frac{r}{a} - \ln k\right) &< \frac{3-\nu}{1-\nu}\ln\frac{1-\nu}{3-\nu}\frac{24\pi\gamma_{\mathrm{SF}}}{Ga}. \end{aligned} \tag{2.24}$$

For simplicity, we may assume $\nu = 1/3$ and $r = 2r_0 \approx 4.33a$. We define two quantities,

$$C = \frac{\gamma_{\mathrm{APB}}^{1\bar{1}0}}{Ga} \tag{2.25}$$

$$\delta = \frac{\gamma_{\mathrm{SF}}^{1\bar{1}0}}{\gamma_{\mathrm{APB}}^{1\bar{1}0}}, \tag{2.26}$$

so that Eq. (2.24), which specifies whether APB formation is more favorable than SF formation, can be rewritten as

$$\ln\delta > -2.132 - \frac{1}{4}\ln C. \tag{2.27}$$

Note that Eq. (2.22) is now equivalent to

$$\ln C > \ln\frac{3}{8\pi ke}. \tag{2.28}$$

For a B2 material to exhibit enhanced ductility, it must possess multiple slip during plastic flow. Thus, the necessary condition for ductility is that APBs must be metastable (Eq. (2.27)), so that $\langle 111\rangle$ slip is possible; yet $\langle 001\rangle$ slip also has to be favorable (Eq. (2.28)).

2.1.2 Sufficient condition: APB$\{1\bar{1}0\}$ and APB$\{11\bar{2}\}$ bistability

As mentioned earlier, $\langle 111\rangle$ APBs can exist on both $\{1\bar{1}0\}$ and $\{11\bar{2}\}$ planes. A ductile B2 material can have multiple slip only if the APB is bistable. Based on the work of Hirth and Lothe [24] and Head [25], the dissociation of $\langle 111\rangle$ screw superdislocations in B2 materials was analyzed in detail by Saada and Veysseiere [18]. Their work was expanded by Sun [26]. Figure 2.2 shows the stability map of the dissociation of $\langle 111\rangle$ APBs on the $\{1\bar{1}0\}$ and $\{11\bar{2}\}$

planes, where the central bistability region is bounded by $2/\sqrt{3}$ and $\sqrt{3}/2$ [26].

We now have three criteria. First, Eq. (2.28) is used for the prediction of $\langle 111 \rangle$ versus $\langle 001 \rangle$ slip. Second, Eq. (2.27) compares the relative stability of APB$\{1\bar{1}0\}$ and SF$\{1\bar{1}0\}$. Finally, multiple slip in $\{1\bar{1}0\}$ and $\{11\bar{2}\}$ via APB formation is governed by the map shown in Figure 2.2. If the necessary condition is fulfilled, i.e., APBs are stable relative to SFs, while $\langle 001 \rangle$ slip is still possible, then the sufficient condition can be used to check whether the material possesses bistability of APBs and hence multiple slip. These criteria will be used to explain the enhanced ductility in RM compounds. Before we proceed, we need to define certain quantities of interest.

2.2 Parameters for B2 systems

To construct stability maps based on the three criteria described in the previous section, elastic constants c_{ij}, APB energies $\gamma^{1\bar{1}0}_{\mathrm{APB}}$ and $\gamma^{11\bar{2}}_{\mathrm{APB}}$, SF energies $\gamma^{1\bar{1}0}_{\mathrm{SF}}$, and various ratios based on these quantities are required. We shall define these quantities in this section.

2.2.1 Lattice constant and bulk modulus

Since B2 is cubic (Fig. 1.1), only one lattice parameter a is needed. To calculate the lattice constant, first note that pressure is related to energy via

$$P = -\frac{\partial E}{\partial V}. \tag{2.29}$$

At the theoretical lattice constant a_0, then,

$$P(a_0) = -\frac{\partial E}{\partial V}\Big|_{a_0^3} = 0. \tag{2.30}$$

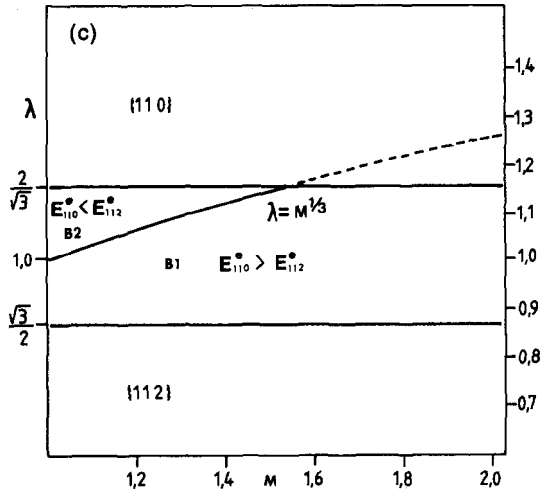

Figure 2.2: Stability map of APB-dissociated $\langle 111 \rangle$ dislocations in B2 systems. (Reprinted from Acta Metall. Mater., 43, Y. Q. Sun, Stability of APB-dissociated $\langle 111 \rangle$ screw superdislocations in B2-ordered structures, 3775–3782, © 1995, with permission from Elsevier.) The map represents the sufficient condition for APB bistability on $\{1\bar{1}0\}$ and $\{11\bar{2}\}$ planes, giving multiple slip modes along $\langle 111 \rangle$.

Thus, a_0 can be found by minimizing the total energy via a least squares fit with a cubic polynomial, since the second derivative is needed to calculate the bulk modulus:

$$B = V\frac{\partial^2 E}{\partial V^2}. \tag{2.31}$$

In B2 systems, it can be shown that (see Appendix B)

$$B = \frac{1}{9a_0}\frac{\partial^2 E}{\partial a^2}\bigg|_{a_0}. \tag{2.32}$$

2.2.2 Elastic constants

The stiffness tensor c_{ijkl} can be written in contracted matrix notation, which has a sparse format due to the symmetry in cubic materials:

$$c_{ij} = \begin{bmatrix} c_{11} & c_{12} & c_{12} & 0 & 0 & 0 \\ c_{12} & c_{11} & c_{12} & 0 & 0 & 0 \\ c_{12} & c_{12} & c_{11} & 0 & 0 & 0 \\ 0 & 0 & 0 & c_{44} & 0 & 0 \\ 0 & 0 & 0 & 0 & c_{44} & 0 \\ 0 & 0 & 0 & 0 & 0 & c_{44} \end{bmatrix}. \tag{2.33}$$

The c_{ij}'s are known as elastics constants, which determine how a crystal deforms under an applied stress. c_{11} is related to the deformation along the direction of a tensile/compressive stress. Due to the Poisson effect, c_{12} describes the deformation perpendicular to the stress. For isotropic cubic materials, c_{44} is equal to the shear modulus G. In practice, the elastic constants c_{11} and c_{12} can be found by solving the system of linear equations:

$$B = \frac{1}{3}(c_{11} + 2c_{12}) \tag{2.34a}$$

$$c' = \frac{1}{2}(c_{11} - c_{12}). \tag{2.34b}$$

c' can be obtained by applying the distortion [27]

$$\begin{bmatrix} 1+\varepsilon & 0 & 0 \\ 0 & 1-\varepsilon & 0 \\ 0 & 0 & \dfrac{1}{1-\varepsilon^2} \end{bmatrix}. \tag{2.35}$$

The associated change in total energy is a function of the strain ε [27]:

$$\frac{\Delta E}{V} = 2c'\varepsilon^2 + O(\varepsilon^4). \tag{2.36}$$

Thus, c' is found by a least squares fit to a quadratic polynomial. Similarly, for c_{44}, one can apply the distortion [27]

$$\begin{bmatrix} 1 & \varepsilon & 0 \\ \varepsilon & 1 & 0 \\ 0 & 0 & \dfrac{1}{1-\varepsilon^2} \end{bmatrix}, \tag{2.37}$$

and

$$\frac{\Delta E}{V} = 2c_{44}\varepsilon^2 + O(\varepsilon^4). \tag{2.38}$$

The Poisson ratio can be computed from

$$\nu = \frac{3B - 2G}{6B + 2G}. \tag{2.39}$$

For metals, ν is typically around 1/3 [20], a value used in the generic derivation of the necessary condition for multiple slip in B2 materials in Section 2.1.1. It is easy to show that $\nu = c_{12}/(c_{11} + c_{12})$ for isotropic materials.

2.2.3 λ and M in sufficient condition

The stability map for $\langle 111 \rangle$ APBs is shown earlier in Figure 2.2, where

$$\lambda = \frac{\gamma_{\mathrm{APB}}^{11\bar{2}}}{\gamma_{\mathrm{APB}}^{1\bar{1}0}} \tag{2.40}$$

is a ratio of APB energies and M is a function of elastic constants, defined as follows [24]. Let $H = 2c_{44} + c_{12} - c_{11}$. A rotation to the [111] axis yields

$$c'_{ij} = \begin{bmatrix} c'_{11} & c'_{12} & c'_{13} & 0 & c'_{15} & 0 \\ c'_{12} & c'_{11} & c'_{13} & 0 & -c'_{15} & 0 \\ c'_{13} & c'_{13} & c'_{33} & 0 & 0 & 0 \\ 0 & 0 & 0 & c'_{44} & 0 & -c'_{15} \\ c'_{15} & -c'_{15} & 0 & 0 & c'_{44} & 0 \\ 0 & 0 & 0 & -c'_{15} & 0 & c'_{66} \end{bmatrix}, \tag{2.41}$$

where

$$\begin{aligned} c'_{11} &= c_{11} + \frac{1}{2}H && \text{(2.42a)} \\ c'_{12} &= c_{12} - \frac{1}{6}H && \text{(2.42b)} \\ c'_{13} &= c_{12} - \frac{1}{3}H && \text{(2.42c)} \\ c'_{33} &= c_{11} + \frac{2}{3}H && \text{(2.42d)} \\ c'_{44} &= c_{44} - \frac{1}{3}H && \text{(2.42e)} \\ c'_{66} &= c_{44} - \frac{1}{6}H && \text{(2.42f)} \\ c'_{15} &= -\frac{\sqrt{2}}{6}H. && \text{(2.42g)} \end{aligned}$$

Note that $H = (c_{11} - c_{12})(A - 1)$, where A is defined in Eq. (1.1). Hence, for an isotropic material, $A = 1$, $H = 0$, and $c'_{ij} = c_{ij}$. The third row and column are deleted to obtain the

inverse [25]:

$$\begin{bmatrix} S_{11} & S_{12} & 0 & S_{15} & 0 \\ S_{12} & S_{11} & 0 & -S_{15} & 0 \\ 0 & 0 & S_{44} & 0 & -2S_{15} \\ S_{15} & -S_{15} & 0 & S_{44} & 0 \\ 0 & 0 & -2S_{15} & 0 & S_{66} \end{bmatrix},$$

where

$$S_{11} = \frac{c'_{11}c'_{44} - c'^2_{15}}{2(c'_{11} + c'_{12})(c'_{44}c'_{66} - c'^2_{15})} \tag{2.43a}$$

$$S_{12} = -\frac{c'_{12}c'_{44} + c'^2_{15}}{2(c'_{11} + c'_{12})(c'_{44}c'_{66} - c'^2_{15})} \tag{2.43b}$$

$$S_{44} = \frac{c'_{66}}{c'_{44}c'_{66} - c'^2_{15}} \tag{2.43c}$$

$$S_{66} = \frac{c'_{44}}{c'_{44}c'_{66} - c'^2_{15}} \tag{2.43d}$$

$$S_{15} = -\frac{c'_{15}}{2(c'_{44}c'_{66} - c'^2_{15})}. \tag{2.43e}$$

Finally, the parameter M is defined as

$$M = \sqrt{\frac{S_{11}S_{44}}{S_{11}S_{44} - S_{15}^2}}. \tag{2.44}$$

As discussed by Sun [26], $M \geq 1$, where the equality holds only for isotropic materials.

Chapter 3

Calculation Methods

Density-functional calculations were performed using the Vienna Ab-initio Simulation Package (VASP) [28, 29, 30]. Ultra-soft pseudopotentials with the projected augmented wave (PAW) basis [31, 32] and the generalized gradient approximation (GGA) to the exchange-correlation functional [33, 34] were used. The k-point mesh was chosen using a method developed by Monkhorst and Pack [35].

Lattice constants and elastic constants were calculated for 2-atom B2 unit cells (Fig. 1.1) with $20\times20\times20$ k-points. For all systems, total energies and forces were converged below 0.1 meV/cell and 0.1 meV/Å, respectively. Elastic constants were calculated at both theoretical (a_0) and experimental lattice constants (a_{expt}). Due to errors in GGA exchange-correlation functionals, metal lattice constants are overestimated, which particularly affect calculations of elastic constants and defect energies. For example, using a lattice constant larger than the experimental value separates the defect planes farther apart and lowers the defect energy, resulting in material-dependent systematic errors. Therefore, a_{expt} was used for calculated properties to remove systematic errors. (See Ref. [36] and references therein for discussion.)

APBs and SFs on the $\{1\bar{1}0\}$ plane were separated by 8 layers of atoms (Fig. 3.1), whereas APB$\{11\bar{2}\}$'s were separated by 6 layers (Fig. 3.2). Each unit cell contained 2 defect planes, so that orthogonal translation vectors could be used as coordinate axes along the defect

plane. Specifically, the translation vectors were

$$\frac{1}{a}\begin{bmatrix}\mathbf{T_1}\\ \mathbf{T_2}\\ \mathbf{T_3}\end{bmatrix} = \begin{cases} \begin{bmatrix} -1 & 1 & 0\\ 0 & 0 & 1\\ 8 & 8 & 0\end{bmatrix} & \text{APB}\,\{1\bar{1}0\}\,,\ \text{SF}\,\{1\bar{1}0\} \\ & \\ \begin{bmatrix} -1 & 1 & 0\\ -1 & -1 & 1\\ 2 & 2 & 4\end{bmatrix} & \text{APB}\,\{11\bar{2}\} \end{cases} . \tag{3.1}$$

The planar defect energies were computed from

$$\gamma = \frac{E_{\text{def}} - E_{\text{perfect}}}{2||\mathbf{T_1} \times \mathbf{T_2}||}, \tag{3.2}$$

where the factor of 2 in the denominator is due to the presence of 2 defect planes per unit cell, see Figures 3.1 and 3.2. In order to remove systematic errors for k-point meshes, the perfect unit cell had the same number of atoms and cell shape as the defected cell. In defected cells, two layers of atoms on each side of the defect plane were relaxed along $\mathbf{T_3}$, with the cell shape and volume fixed (for reasons stated above). The planar defect energies of APB$\{1\bar{1}0\}$ and SF$\{1\bar{1}0\}$ were calculated for 32-atom unit cells at a_{expt}, with at least $12\times12\times2$ k-points. In calculating the planar defect energy of APB$\{11\bar{2}\}$, $8 \times 8 \times 4$ k-points were used, with 24 atoms in the unit cell. The k-point meshes were chosen such that the reciprocal axes contained a similar density of k-points. The aspect ratio in k-space, then, was roughly the reciprocal of that in real space. Using more k-points, such as $12 \times 12 \times 4$ and $16 \times 16 \times 4$ in APB$\{1\bar{1}0\}$ and $12 \times 12 \times 8$ in APB$\{11\bar{2}\}$, did not affect the results (see Table 3.1).

We note that along with APBs and SFs, high-symmetry twins may also be energetically favorable. The twin$\{11\bar{2}\}$ defect energy in NiAl is $2\gamma_{\text{twin}}^{11\bar{2}} = 874$ mJ/m^2, comparable to the APB energies in Table 3.1.

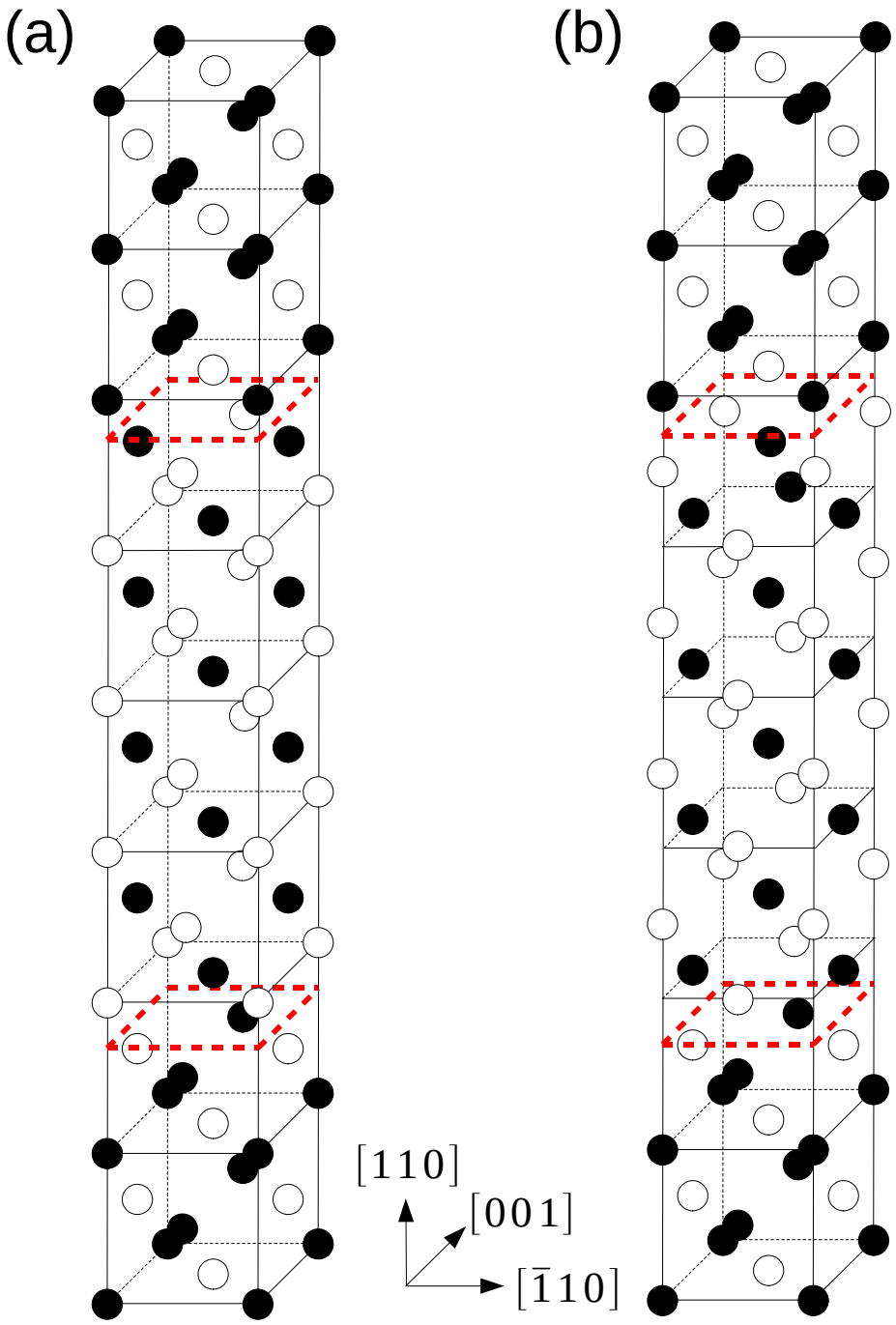

Figure 3.1: Unit cells of (a) APB$\{1\bar{1}0\}$ (after Ref. [37]) and (b) SF$\{1\bar{1}0\}$ used in the present work. Filled and open circles represent different atomic species. The two defect planes per unit cell are dashed in red.

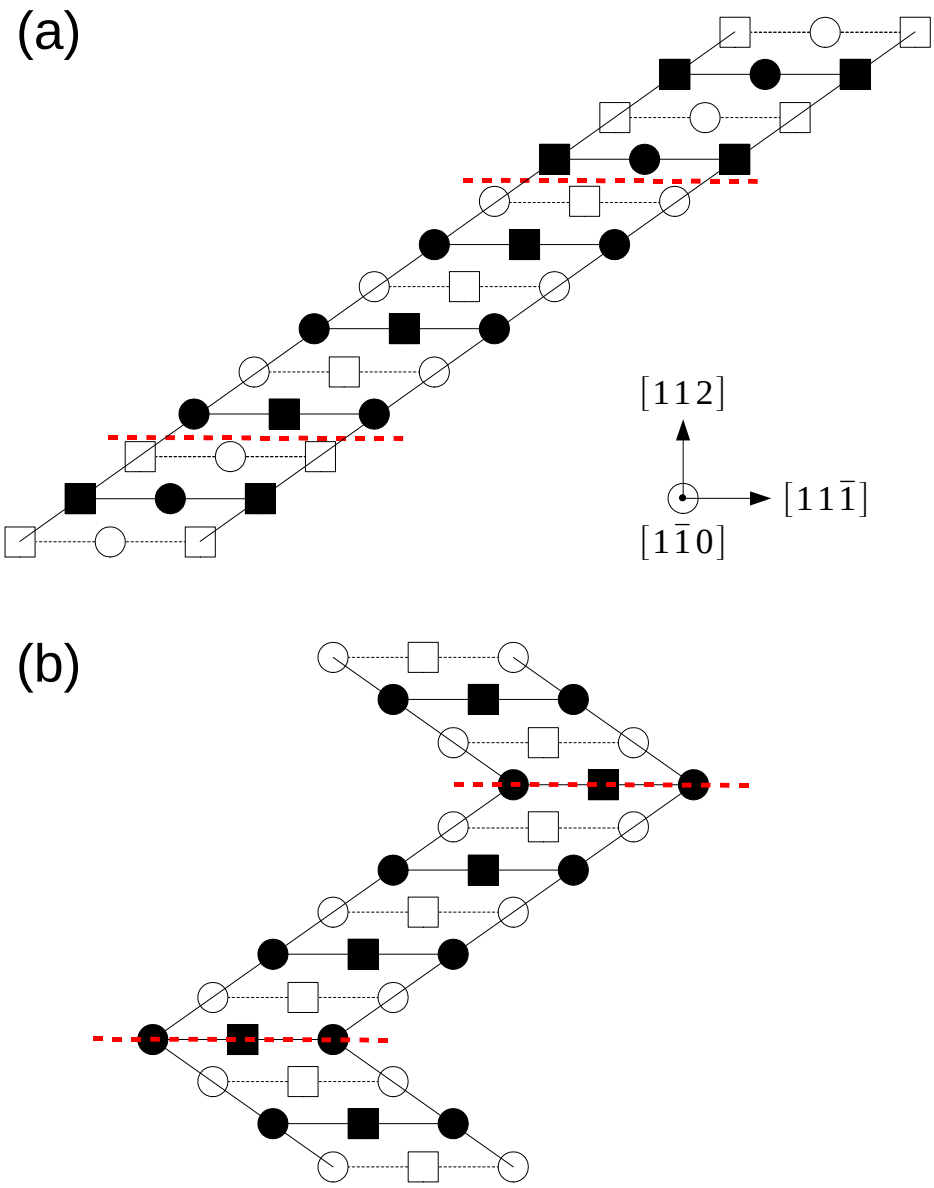

Figure 3.2: Projection of (a) APB(112) and (b) twin(112) unit cells onto the $(1\bar{1}0)$ plane. Circles and rectangles represent the two atomic species. Filled symbols represent atoms in the plane; open symbols represent atoms $\frac{a}{2}[1\bar{1}0]$ behind the plane. The two defect planes per unit cell are dashed in red.

Table 3.1: Comparison of using different k-point meshes for calculating APB energies. E_{perfect} and E_{def} are the energies of the perfect and defected unit cells, respectively. (E in eV/cell; γ_{APB} in mJ/m^2.)

Defect	Material	k-point mesh	E_{perfect}	E_{def}	γ_{APB}
APB$\{1\bar{1}0\}$	YAg	$12 \times 12 \times 2$	-157.215	-155.734	641
		$12 \times 12 \times 4$	-157.216	-155.735	641
	YCu	$12 \times 12 \times 2$	-169.988	-168.373	757
		$12 \times 12 \times 4$	-169.988	-168.373	757
		$16 \times 16 \times 4$	-169.984	-168.372	755
APB$\{11\bar{2}\}$	YAg	$8 \times 8 \times 4$	-117.918	-114.979	734
		$12 \times 12 \times 8$	-117.915	-114.982	732
	YCu	$8 \times 8 \times 4$	-127.491	-124.049	931
		$12 \times 12 \times 8$	-127.489	-124.051	930
	YIn	$8 \times 8 \times 4$	-119.421	-117.036	549
		$12 \times 12 \times 8$	-119.422	-117.036	549

Chapter 4

Results and Discussion

As discussed in Chapter 2, there are two central issues being addressed for B2 systems:

1. What are the dominant slip systems predicted via mesoscale dislocation mechanics? Are the $\langle 111 \rangle$ APBs more energetically favorable than SFs? These determine the necessary condition for ductility.

2. Are the $\langle 111 \rangle \{1\bar{1}0\}$ and $\langle 111 \rangle \{11\bar{2}\}$ slip systems jointly active for enhanced ductility? This gives the sufficient condition.

The necessary condition is governed by Eqs. (2.27) and (2.28). The sufficient condition is shown in Figure 2.2. APB and SF planar defect energies as well as structural and elastic constant information are required as input. Specifically, the ratios $C = \gamma^{1\bar{1}0}_{\mathrm{APB}}/(Ga)$ and $\delta = \gamma^{1\bar{1}0}_{\mathrm{SF}}/\gamma^{1\bar{1}0}_{\mathrm{APB}}$ are used in the necessary condition; $M = \sqrt{S_{11}S_{44}/(S_{11}S_{44} - S_{15}^2)}$ and $\lambda = \gamma^{11\bar{2}}_{\mathrm{APB}}/\gamma^{1\bar{1}0}_{\mathrm{APB}}$ are used in the sufficient condition. Here we present calculation results for lattice constants and elastic constants with experimental values. We then show the APB and SF energies and plot the stability maps. The atypical ductility of the Y-based compounds will be discussed. For most materials, the calculated structural parameters and the predicted slip directions show excellent agreement with experimental results, as detailed below.

4.1 Lattice Constants and Elastic Parameters

The calculated lattice constants are listed in Table 4.1. It is well known that the GGA overestimates the lattice constants for metals [36]. Since the a_{expt}'s are measured at room

temperature, whereas the a_0's are obtained at zero Kelvin, it is more appropriate to extrapolate the $a_{\rm expt}$'s to 0 K, making the error in the GGA exchange-correlation results even larger. Alternatively, one can include phonon contributions to find a_0 at room temperature. Due to thermal expansion, we expect a_0 to increase, again showing the large discrepancy between a_0 and $a_{\rm expt}$. However, as discussed in Chapter 3, the experimental lattice and elastic constants are used to provide a better estimate of defect energies, allowing us to determine the location of each system in the stability maps more accurately. Since $a_{\rm expt}$ of YIn is unknown, all of its parameters are calculated at a_0, which can alter slightly its position in the maps.

From Table 4.1, we see that the differences between a_0 and $a_{\rm expt}$ for the systems investigated have a range from -0.2% for YMg, 0.2% for YCu, 1.0% for YRh, 1.8% for CsCl, to 2.3% for AuCd. (As noted below, AuCd is the only system that has large discrepancies with the experimental structural parameters, B, c', c_{44}, A, ν, and M. Further investigation of the issue is required to understand its origin.) As a specific example, in Figure 4.1(a) we show the energy versus lattice constant plot for NiAl. Minimization yields $a_0 = 2.895$ Å at 0 K. Compared to $a_{\rm expt} = 2.886$ Å at room temperature, there is a 0.3% difference between theory and experiment.

The theoretical values for B, c', and c_{44} evaluated at the experimental lattice constant are slightly different from reported values. For example, the error in the calculated B ranges from 0.0% for NiAl, 7.1% for YAg, to 53.9% for AuCd (which is the single most discrepant system, due to the sensitivity in the lattice constant). Using Eqs. (2.34a) and (2.34b), c_{11} and c_{12} are calculated from B and c' listed in Table 4.1. As an example, in Figure 4.1(b) we show the energy change versus strain for NiAl. Fitting the energy difference as a function of strain yields $c' = 39.5$ GPa and $c_{44} = 116.5$ GPa at 0 K; the observed values at room temperature are 34.2 GPa and 112.1 GPa, respectively. Given c_{11}, c_{12}, and c_{44}, we can then determine the Zener anisotropy ratio A (Eq. (1.1)), the Poisson ratio ν (Eq. (2.39)), and the important elastic constant ratio M (Eq. (2.44)).

The critical parameters for the sufficient condition map are λ, a ratio of defect energies

(Eq. (2.40)), and M (Eq. (2.44)). In YAg, M is calculated to be 1.02, the same as the experimental value; A is 1.67 (experiment 1.54), indicating an anisotropic system. As for YCu, which, as we will show, is less ductile than YAg, we find $M = 1.00$ (experiment 1.00) and $A = 1.08$ (experiment 0.99), showing YCu is much more elastically isotropic. It is worthwhile to point out that $A < 1$ in the ionic B2 systems (e.g., CsCl has $M = 1.01$ and $A = 0.69$), which means that these materials exhibit anisotropy with deformation behaviors different from those of the metallic systems. For most systems, M has an error of 2%. (The worst calculation is in AuCd, where the error in M is 58%. The reason for such a huge discrepancy is unclear.) As opposed to YAg, YCu, and YRh, our results show that YIn and YMg are highly anisotropic. Further investigation is necessary to understand the inherent differences between these sets of systems, for example, from changes in electron densities under shear.

From examination of Table 4.1, as expected, the elastic constants and other structural parameters calculated at a_{expt} show significant improvement compared to those calculated at a_0, agreeing with experimental values within the known errors of GGA, save AuCd. We now use these calculated values to investigate the stability of the possible operative slip systems for the B2 materials.

Table 4.1: Calculated and experimental lattice constants (in Å), bulk moduli (in GPa), and elastic constants (in GPa) of B2 materials. A, ν, and M are defined in Eqs. (1.1), (2.39), and (2.44), respectively. In the first (second) row of each system, calculations were performed at a_0 (a_{expt}). References for a_{expt} are given in the second row. In the third row, B, c', A, ν, and M were calculated from the experimental elastic constants.

Material	a	B	c'	c_{11}	c_{12}	c_{44}	A	ν	M	Ref.
YAg	3.646	68.3	22.3	98.0	53.4	35.0	1.57	0.281	1.02	
	3.619	75.1	22.6	105.2	60.0	37.8	1.67	0.284	1.02	[12]
	3.619	70.1	24.2	102.4	54.0	37.2	1.54	0.276	1.02	[12]
YCu	3.485	71.3	34.4	117.2	48.4	36.4	1.06	0.282	1.00	
	3.477	73.4	34.6	119.6	50.3	37.2	1.08	0.283	1.00	[12]
	3.477	70.1	32.5	113.4	48.4	32.3	0.99	0.300	1.00	[12]
YIn	3.769	57.3	6.02	65.3	53.3	43.4	7.20	0.198	1.35	
YRh	3.442	113.3	38.4	164.5	87.7	36.6	0.95	0.354	1.00	
	3.407	121.2	38.0	171.8	95.9	40.4	1.06	0.350	1.00	[39]
YMg	3.798	41.2	8.62	52.7	35.5	39.6	4.60	0.136	1.19	
	3.806	40.4	8.55	51.8	34.7	39.1	4.57	0.134	1.18	[40]
NiAl	2.895	159.4	38.4	210.5	133.8	112.8	2.94	0.214	1.10	
	2.886	166.0	39.5	218.7	139.6	116.5	2.95	0.216	1.10	[38]
		166.0	34.2	211.6	143.2	112.1	3.28	0.224	1.12	[41]
FeAl	2.879	161.3	52.8	231.6	126.1	130.2	2.47	0.182	1.06	
	2.909	156.4	51.7	225.4	121.9	123.5	2.39	0.187	1.06	[38]
		136.1	33.7	181.1	113.7	127.1	3.77	0.144	1.14	[41]
AuCd	3.398	93.0	1.31	94.7	92.1	37.4	28.8	0.323	2.41	
	3.323	130.8	1.58	132.9	129.8	56.1	36.2	0.312	2.66	[38]
		85	3.5	90	83	44	12.6	0.279	1.68	[18]
AuZn	3.195	116.9	5.72	124.5	113.1	42.8	7.47	0.337	1.42	
	3.149	145.4	7.31	155.2	140.5	55.7	7.62	0.330	1.42	[42]
	3.149	131.5	7.73	141.8	126.3	54.52	7.04	0.318	1.38	[42]
CuZn	2.969	113.8	7.67	124.0	108.7	78.6	10.2	0.219	1.53	
	2.954	122.6	8.00	133.3	117.3	83.5	10.4	0.222	1.54	[38]
		116.2	9.70	129.1	109.7	82.4	8.50	0.213	1.43	[43]
AgMg	3.331	65.9	13.4	83.8	57.0	47.1	3.51	0.212	1.13	
	3.314	70.9	14.2	89.8	61.5	49.7	3.51	0.216	1.13	[38]
		65.6	13.7	83.8	56.4	47.6	3.46	0.208	1.13	[41]

Continued on next page ...

Table 4.1 (cont'd)

Material	a	B	c'	c_{11}	c_{12}	c_{44}	A	ν	M	Ref.
CsCl	4.196	15.0	11.0	29.6	7.65	5.24	0.48	0.344	1.04	
	4.120	19.3	11.6	34.7	11.6	8.03	0.69	0.317	1.01	[44]
		18.2	14.0	36.6	8.82	8.04	0.58	0.307	1.02	[41]
CsI	4.656	10.0	7.01	19.4	5.37	4.20	0.60	0.316	1.02	
	4.567	13.2	7.54	23.3	8.21	6.56	0.87	0.287	1.00	[44]
		12.7	8.95	24.6	6.70	6.24	0.70	0.289	1.01	[41]
TlBr	4.011	22.1	12.6	38.9	13.7	6.21	0.49	0.372	1.04	
	3.986	24.4	12.7	41.3	15.9	7.51	0.59	0.360	1.02	[45]
		22.4	11.2	37.3	14.0	7.48	0.67	0.350	1.01	[41]
TlCl	3.855	25.6	14.5	44.9	16.0	7.11	0.49	0.373	1.04	
	3.842	27.0	14.5	46.4	17.3	7.86	0.54	0.367	1.03	[45]
		23.6	12.4	40.1	15.3	7.60	0.61	0.355	1.02	[41]

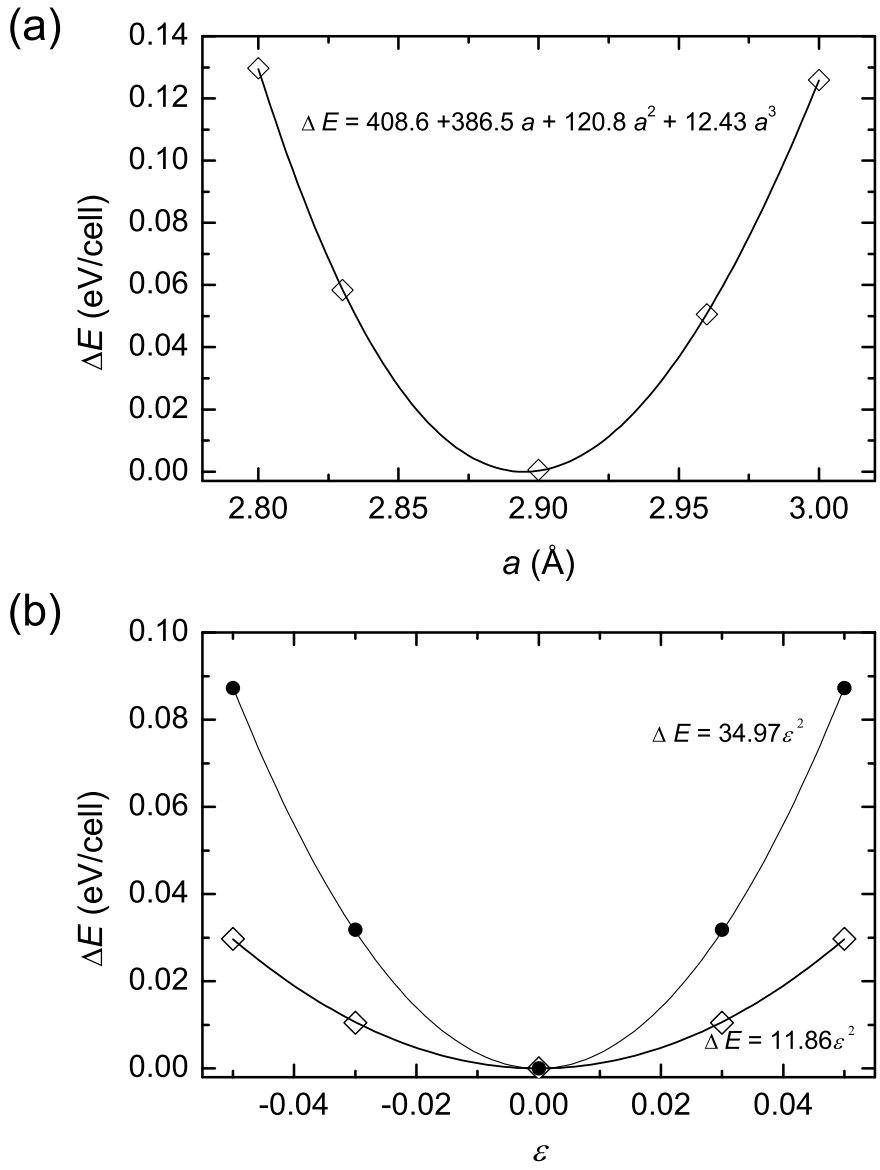

Figure 4.1: Calculation of a_0, c', and c_{44} in NiAl. (a) a_0 is found by minimizing the energy as with respect to B2 lattice constant. A cubic polynomial is used to fit the data. Here $\Delta E(a) = E(a) - E(a_0)$, where $E(a_0) = -10.4988$ eV/cell. (b) Diamonds and circles represent the increase in energy by applying the distortions in Eqs. (2.35) and (2.37), respectively. c' and c_{44} can then be determined from Eqs. (2.36) and (2.38). The energies are calculated at a_{expt}, so $\Delta E(\varepsilon) = E(\varepsilon) - E(a_{\text{expt}})$, where $E(a_{\text{expt}}) = -10.4978$ eV/cell.

4.2 Stability Maps

4.2.1 Necessary condition

The APB and SF energies are listed in Table 4.2. Using Eq. (2.28) and data from Table 4.2, we may construct a stability map for the energetically preferred slip directions in B2 materials, as shown in Figure 4.2. Taking $k \approx 2.17$ in Eq. (2.28), we see that $\langle 001 \rangle$ slip is more favorable for systems lying to the right of the vertical line, whereas to the left $\langle 111 \rangle$ slip is favored. The predicted and experimentally observed slip systems are compared in Table 4.3. Systems favoring $\langle 001 \rangle$ slip include YAg, YCu, YIn, YRh, NiAl, and all the CsCl-type ionic compounds. CuZn and FeAl fall on the left-hand side of the vertical line, showing that $\langle 111 \rangle$ slip is favorable, which agrees with the experimental observation of exclusive $\langle 111 \rangle$ slip in these two materials [7, 8, 46, 47, 48]. AgMg lies in the middle region between the estimated boundaries (vertical lines of k ranging from 2.17 to 4.33). Interestingly, both $\langle 111 \rangle$ [7] and $\langle 001 \rangle$ slip directions [49] have been observed in AgMg, with a transition from $\langle 111 \rangle$ to $\langle 001 \rangle$ slip at low temperatures [5].

Apparently, there are two discrepancies between theory and experiment. (1) AuCd is predicted to exhibit $\langle 111 \rangle$ slip; yet $\langle 001 \rangle$ is the only slip direction observed in AuCd. However, as already noted in the previous section, the errors in calculating the lattice and elastic constants in AuCd are significant; hence, the accuracy and reliability of the calculated quantities required for the maps (M, C, APB and SF energies, etc.) may have been greatly affected. (2) There is an ambiguity in the prediction for AuZn, whereas only $\langle 001 \rangle$ slip has been observed [7, 49]. It is unclear why our predictions are unsatisfying for the Au-based B2 materials. Among the rest, our simple model predicts $\langle 001 \rangle$ versus $\langle 111 \rangle$ slip accurately.

In Figure 4.2, we compare the relative stability of SF$\{1\bar{1}0\}$ and APB$\{1\bar{1}0\}$ along with the expected dominant slip direction. The Poisson ratio of all investigated systems are roughly between 1/5 and 1/3. For convenience, the boundary between APB and SF is constructed assuming a generic value of $\nu = 1/3$ to simplify Eq. (2.27). Using $\nu = 1/5$ (not shown),

the small shift in the boundary line does not affect the analysis hereafter. For the ionic compounds, SFs are more stable than APBs, which is expected because $\langle 001 \rangle$ slip direction results in minimum charge repulsion. On the other hand, APBs are relatively stable in both the Y-based compounds and the classic B2 alloys.

However, for systems with metastable APBs, only those in the upper-right quadrant of Figure 4.2 satisfy the *necessary* condition for ductility. In this quadrant, $\langle 001 \rangle$ slip is favorable, but SFs are not stable, which means that $\frac{1}{2}\langle 111 \rangle$ partial dislocations can coexist with the $\langle 111 \rangle$-dissociated perfect $\langle 001 \rangle$ dislocations. Indeed, it has been reported that $\langle 111 \rangle$ dislocations are metastable in NiAl [50] and that they have been observed in the Y-based compounds [1]. This is the first central result: the stability map in Figure 4.2 identifies candidates for multiple slip, and only a subset of Y-based B2 systems and some others qualify.

4.2.2 Sufficient condition

The *necessary* condition alone cannot predict ductility. The *sufficient* condition—whether the APBs are bistable—must be verified. Candidates for ductility are YAg, YCu, YIn, YRh, NiAl, and CsI. In Figure 4.3, we show the condition for multiple slip in B2 materials. Systems that do not satisfy the necessary condition are included for comparison. Only YAg and YRh possess $\{1\bar{1}0\}$ and $\{11\bar{2}\}$ bistability, with YCu being marginal, as it is near the boundary, while YIn, NiAl, and CsI lie away from the bistability region. The bistability of APBs explains the observation of many $\langle 111 \rangle$ dislocations in the Y-based compounds [1], even though $\langle 001 \rangle$ is the dominant slip direction.

Hence, combining $\langle 111 \rangle$ APB bistability with feasibility of $\langle 001 \rangle$ slip, dislocation dissociation resulting in multiple slip is highly favorable in YAg and YRh, but not in other B2 materials. The fact that YCu possesses only half as many slip modes as YAg and YRh shows YCu should be roughly half as ductile as YAg and YRh, which is observed in Figure 1.2 [1].

Table 4.2: Calculated APB and SF energies (in mJ/m^2) of B2 materials. The dimensionless parameters λ, C, and δ are defined in Eqs. (2.40), (2.25), and (2.26), respectively. Present calculation results are listed on the first row of each system. Other calculation results of γ_{APB} and γ_{SF} are provided, if available.

Material	$\gamma_{\mathrm{APB}}^{110}$	$\gamma_{\mathrm{APB}}^{112}$	λ	w_{APB}^{110}/a	C	Ref.	$\gamma_{\mathrm{SF}}^{110}$	δ	Ref.
YAg	641	732	1.14	2.55	0.0468		364	0.569	
	745	680	0.91	2.16	0.0553	[12]	305	0.409	[14]
YCu	757	931	1.23	2.04	0.0585		322	0.425	
	1030	1090	1.06	1.30	0.0917	[12]	270	0.262	[14]
YIn	366	549	1.50	5.33	0.0224		636	1.740	
							480		[14]
YRh	1270	1390	1.10	1.29	0.0924		626	0.493	
							430		[14]
YMg	277	259	0.93	6.41	0.0186		714	2.58	
NiAl	777	971	1.25	5.17	0.0231		1379	1.77	
	815	995	1.22	4.74	0.0252	[12]	1290	1.58	[12]
	810	990	1.22	4.93	0.0250	[51]			
FeAl	348	403	1.16	12.3	0.0097		1248	3.59	
	300	820	2.73	14.7	0.0081	[51]			
AuCd	187	223	1.19	11.9	0.0101		639	3.41	
AuZn	247	303	1.22	8.47	0.0141		636	2.58	
CuZn	98	124	1.27	30.2	0.0040		1027	10.5	
	50	37	0.74	58.1	0.0021	[52][1]			
			1.09			[53][1]			
AgMg	254	311	1.22	7.73	0.0154		655	2.58	
CsCl	496	659	1.33	0.80	0.1500		85	0.172	
CsI	357	459	1.29	1.00	0.1191		78	0.219	
TlBr	320	397	1.24	1.12	0.1069		49	0.154	
TlCl	369	458	1.24	0.98	0.1221		51	0.137	

[1]Experiment

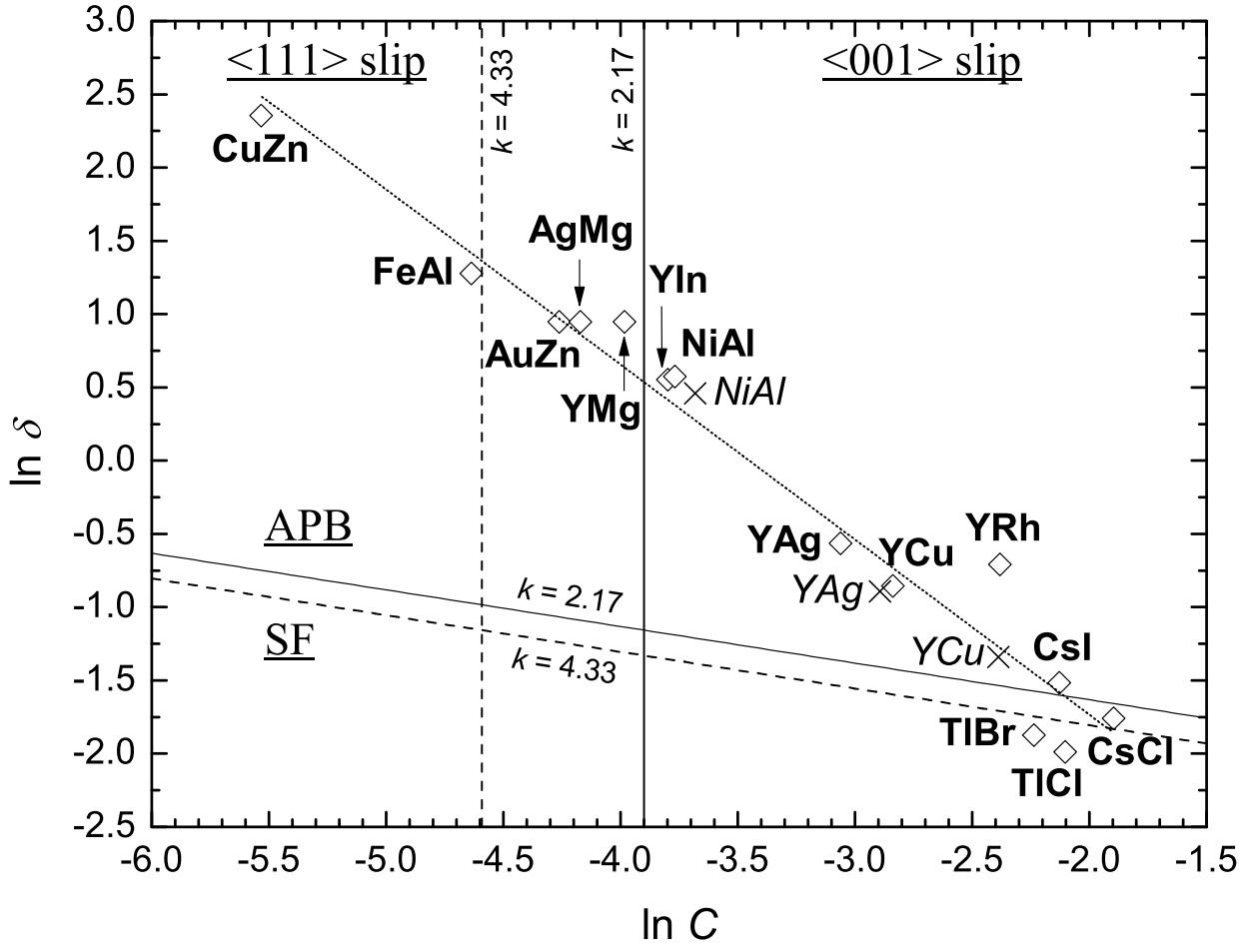

Figure 4.2: Necessary condition map: $\ln \delta$ versus $\ln C$ plot for B2 materials, indicating preferred slip directions and APB/SF stability. Diamonds and bold labels represent the present work; crosses and italic labels are taken from other calculation results listed in Table 4.2. The dotted line through the data is a guide for the eye. The solid (dashed) vertical and slanted lines of slope $-1/4$ correspond to $k \approx 2.17$ (4.33). To the right (left) of the vertical line, $\langle 001 \rangle$ ($\langle 111 \rangle$) slip is more favorable. Above the slanted line of slope $-1/4$, APBs are more energetically stable than SFs, whereas SFs are more stable than APBs below this line. Systems lying in the upper-right quadrant satisfy the necessary condition for ductility.

Table 4.3: Predicted and experimentally observed slip systems (under tensile and compressive loadings) in B2 materials.

Material	Predicted	Observed			
		Tensile	Ref.	Compressive	Ref.
YAg	$\langle 001 \rangle$	RT: $\langle 001 \rangle \{110\}$	[1]		
YCu	$\langle 001 \rangle$	RT: $\langle 001 \rangle \{110\}$, $\langle 001 \rangle \{100\}$	[1]	RT: No slip	[1]
YIn	$\langle 001 \rangle$				
YRh	$\langle 001 \rangle$				
YMg	$\langle 001 \rangle$ or $\langle 111 \rangle$				
NiAl	$\langle 001 \rangle$			$< 0.45T_m$: $\langle 001 \rangle \{1\bar{1}0\}$	[8]
FeAl	$\langle 111 \rangle$	77–1143 K: $\langle 111 \rangle \{1\bar{1}0\}$	[47]	77 K: $\langle 111 \rangle \{11\bar{2}\}$	[48]
				473 K: $\langle 111 \rangle \{1\bar{1}0\}$	[48]
AuCd	$\langle 111 \rangle$	RT: $\langle 001 \rangle \{1\bar{1}0\}$	[7]		
AuZn	$\langle 001 \rangle$ or $\langle 111 \rangle$	$\langle 001 \rangle \{1\bar{1}0\}$	[7]		
		$\langle 001 \rangle \{hk0\}$	[49]		
CuZn	$\langle 111 \rangle$	$\langle 111 \rangle \{1\bar{1}0\}$	[7]	$< 0.45T_m$: $\langle 111 \rangle \{1\bar{1}0\}$	[8]
				RT, 493 K: $\langle 111 \rangle \{11\bar{0}\}$	[46]
AgMg	$\langle 001 \rangle$ or $\langle 111 \rangle$	$\langle 001 \rangle \{hk0\}$, $\langle 111 \rangle \{11\bar{2}\}$	[49]	$\langle 111 \rangle \{11\bar{2}\}$	[49]
		$\langle 111 \rangle \{\bar{3}21\}$	[7]		
CsCl	$\langle 001 \rangle$				
CsI	$\langle 001 \rangle$				
TlBr	$\langle 001 \rangle$			$\langle 001 \rangle \{1\bar{1}0\}$	[54]
TlCl	$\langle 001 \rangle$			$\langle 001 \rangle \{1\bar{1}0\}$	[54]

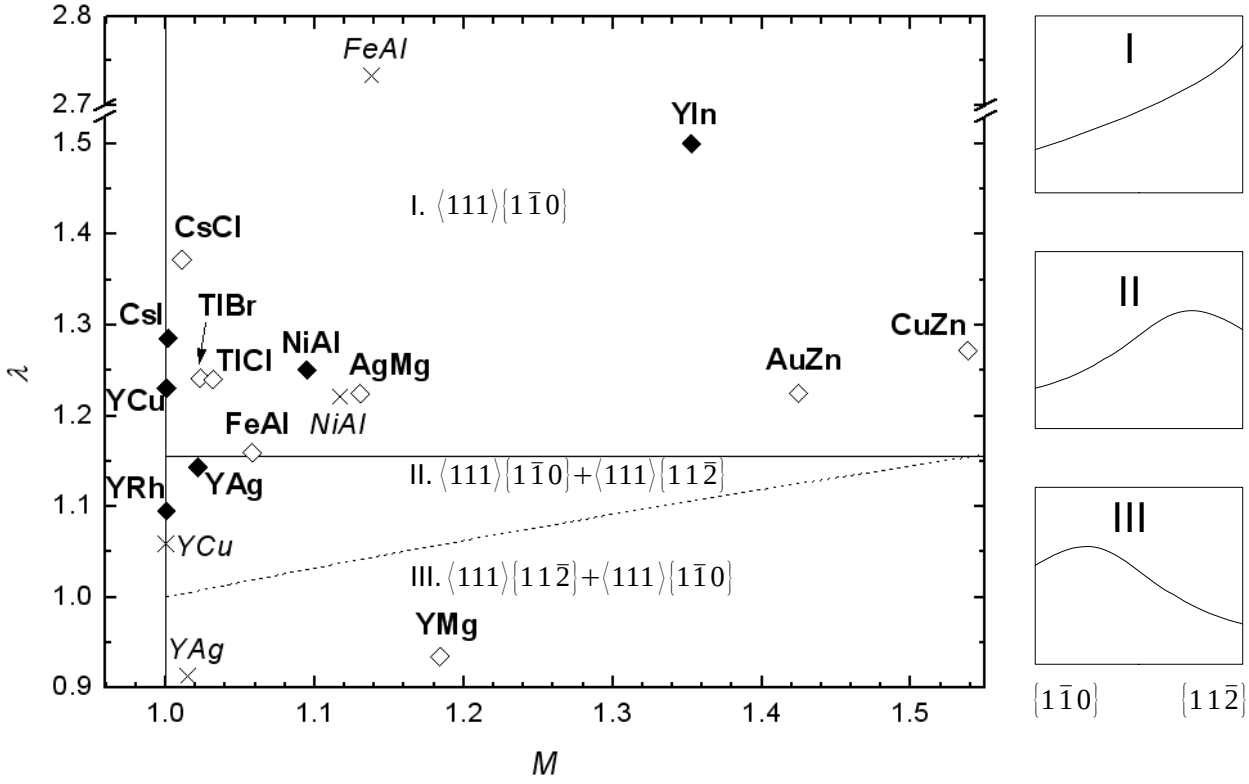

Figure 4.3: Sufficient condition map: λ versus M plot for B2 materials, indicating possibility of multiple slip systems if $\sqrt{3}/2 < \lambda < 2/\sqrt{3}$. Diamonds and bold labels represent the present work; crosses and italic labels are taken from the third rows of Table 4.1 and the second rows of Table 4.2, if both are available. Materials that do not satisfy the *necessary* condition are marked in open diamonds. To the right of the figure are schematics (after Ref. [26]) showing the relative energy of the slip systems for the three regions.

It happens that none of the anisotropic B2 materials satisfy both the necessary and sufficient conditions, explaining the observation of brittleness in all the classic B2 alloys [6]. The ductile materials are all near isotropic. Hence, elastic isotropy may serve as an indicator for enhanced ductility. It is not a quantitative indicator because YCu is more isotropic than YAg, but YCu is less ductile.

Not all Y-based compounds are ductile—YIn does not satisfy the sufficient condition, while YMg does not satisfy the necessary condition. The latter is experimentally confirmed [4]; the former does not agree with the preliminary findings of Gschneidner *et al.* [1], and experimental verification is required. (Also, as seen in Table 4.1, YIn cannot be compared with experiment for it is the only system without empirical data.) Clearly, both necessary and sufficient conditions are required to predict ductility. Finally, we remark that the data in Figure 4.2 lie along a line.

We have provided a set of simple, energy-based stability maps that can be used to *a priori* determine whether B2 materials are ductile, explaining the enhanced ductility observed in RM intermetallic compounds. The same maps can still be used for B2 alloy design, and one may consider temperature effects, point defects, or disorder to construct modified maps for system-specific predictions.

Chapter 5

Conclusions

We have addressed—through solely energy-based criteria—$\langle 001 \rangle$ versus $\langle 111 \rangle$ slip, the relative stability of APBs and SFs, and bistability of APB$\{1\bar{1}0\}$ and APB$\{11\bar{2}\}$, which are the dominant slip modes and defects in B2 systems that can lead to enhanced ductility. Through these criteria, we have constructed two stability maps using mesoscale dislocation mechanics that require only ratios of defect energies and/or elastic constants obtained from first-principles density-functional theory calculations. We have examined 15 B2 materials, including classic B2 alloys like CuZn and NiAl, ionic systems like CsCl, and a set of RM B2 compounds, some of which show dramatically enhanced ductility, comparable to fcc Al. In general, the derived stability maps are able to separate the distinct behavior in the three types of materials, predicting which systems exhibit enhanced ductility. In particular, we find that YAg has multiple operative slip systems, which explains its dramatic ductility compared to standard B2 NiAl or CuZn. The ductility of YCu is predicted to be half that of YAg, as is observed.

For any B2 material, $\langle 001 \rangle$ slip is more favorable than $\langle 111 \rangle$ slip if the width of APB$\{1\bar{1}0\}$ is less than about 6 times the lattice constant. The ductile and non-ductile materials are separated into different regions on the stability maps, indicating typical versus enhanced ductility. We summarize our results for the three types of materials as follows.

(1) For the CsCl-based ionic compounds, only $\langle 001 \rangle$ slip is possible. Thus, the necessary condition for ductility is not satisfied. Even if the borderline CsI were assumed to satisfy the necessary condition, the lack of APB bistability would account for its brittleness.

(2) For the classic B2 alloys, all but NiAl fail the necessary condition. Again, APBs of

NiAl do not possess bistability; hence, multiple slip leading to plastic flow is not possible.

(3) For the Y-based compounds, only YAg and YRh satisfy both the necessary and sufficient conditions without ambiguity. They are predicted to exhibit high ductility, with the former has been reported. YCu has half the number of slip modes as that of YAg, so we predict to be half as ductile, which is also observed. YIn and YMg do not satisfy the sufficient and necessary condition, respectively; they are predicted to be brittle, where the latter is confirmed experimentally.

In closing, we find that an energy-based mesoscale dislocation analysis combined with first-principles calculations characterizes permitted slip modes in B2 systems accurately, and can predict enhanced ductility due to coexistence of $\langle 001 \rangle$ slip and $\langle 111 \rangle$ APBs, and bistability of APBs on $\{1\bar{1}0\}$ and $\{11\bar{2}\}$ planes. The Zener anisotropy ratio can be used to screen candidates for further investigation in stability maps.

Appendix A

Derivation of Necessary Condition in $L1_2$ Systems

On the {111} plane of $L1_2$ systems, there are two possible dissociation mechanisms for a screw superdislocation:

$$a[\bar{1}01] \rightarrow \frac{a}{3}[\bar{2}11] + \text{SISF} + \frac{a}{3}[\bar{1}\bar{1}2] \tag{A.1}$$

$$a[\bar{1}01] \rightarrow \frac{a}{2}[\bar{1}01] + \text{APB} + \frac{a}{2}[\bar{1}01] \tag{A.2}$$

Paidar, Pope, and Yamaguchi [16] gave the condition for the first dissociation process to be more favorable over the second:

$$\ln \frac{8\pi\gamma_{\text{SISF}}}{Ga} < 2 \ln \frac{4\pi\gamma_{\text{APB}}}{Ga} + 1. \tag{A.3}$$

We derive it as follows.

The SISF has both edge and screw components:

$$\frac{a}{3}[\bar{2}11] \rightarrow \underbrace{\frac{a}{2}[\bar{1}01]}_{\mathbf{b}_s} + \underbrace{\frac{a}{6}[\bar{1}2\bar{1}]}_{\mathbf{b}_e}, \tag{A.4}$$

so $b_s^2 = a^2/2$ and $b_e^2 = a^2/6$. The self and interaction energies for screw and edge dislocations are given in Eqs. (2.4)–(2.7). The total energy of SISF formation is

$$E_1 = 2E_s + E_{ss} + 2E_e - E_{ee} + \gamma_{\text{SISF}} w_{\text{SISF}}, \tag{A.5}$$

where w_{SISF} is the stacking fault width. The edge interaction energy is negative because the edge components are antiparallel. The separation width w_{SISF} can be found by minimizing Eq. (A.5):

$$\begin{aligned} 0 = \frac{\partial E_1}{\partial w_{\mathrm{SISF}}} &= -\frac{Gb_s^2}{2\pi w_{\mathrm{SISF}}} + \frac{Gb_e^2}{2\pi(1-\nu)w_{\mathrm{SISF}}} + \gamma_{\mathrm{SISF}} \\ w_{\mathrm{SISF}} &= \frac{G}{2\pi\gamma_{\mathrm{SISF}}}\left(b_s^2 - \frac{b_e^2}{1-\nu}\right) = \frac{Ga^2}{8\pi\gamma_{\mathrm{SISF}}}, \end{aligned} \tag{A.6}$$

where we have assumed $\nu = 1/3$.

Next, for the APB, the total energy is

$$E_2 = 2E_s + E_{ss} + \gamma_{\mathrm{APB}} w_{\mathrm{APB}}. \tag{A.7}$$

The APB width can be found similarly:

$$\begin{aligned} 0 = \frac{\partial E_2}{\partial w_{\mathrm{APB}}} &= -\frac{Gb_s^2}{2\pi w_{\mathrm{APB}}} + \gamma_{\mathrm{APB}} \\ w_{\mathrm{APB}} &= \frac{Ga^2}{4\pi\gamma_{\mathrm{APB}}}. \end{aligned} \tag{A.8}$$

In order for SISF to be energetically favorable over APB, we need $E_1 < E_2$, i.e,

$$\begin{aligned} \frac{Ga^2}{4\pi}\left(\ln\frac{r}{r_0} + \ln\frac{r}{w_{\mathrm{SISF}}}\right) + \frac{Ga^2}{8\pi}\left(\ln\frac{r}{r_0} - \ln\frac{r}{w_{\mathrm{SISF}}}\right) + \frac{Ga^2}{8\pi} &< \frac{Ga^2}{4\pi}\left(\ln\frac{r}{r_0} + \frac{r}{w_{\mathrm{APB}}} + 1\right) \\ \frac{3}{2}\ln\frac{r}{r_0} + \frac{1}{2}\ln\frac{r}{w_{\mathrm{SISF}}} + \frac{1}{2} &< \ln\frac{r}{r_0} + \ln\frac{r}{w_{\mathrm{APB}}} + 1 \\ \ln\frac{r}{w_{\mathrm{SISF}}} &< 2\ln\frac{r}{w_{\mathrm{APB}}} + 1 - \ln\frac{r}{r_0}. \end{aligned}$$

Finally, taking $r_0 = a$, we get

$$\begin{aligned} \ln\frac{a}{w_{\mathrm{SISF}}} &< 2\ln\frac{a}{w_{\mathrm{APB}}} + 1 \\ \ln\frac{8\pi\gamma_{\mathrm{SISF}}}{Ga} &< 2\ln\frac{4\pi\gamma_{\mathrm{APB}}}{Ga} + 1. \end{aligned} \tag{A.9}$$

Appendix B

Derivation of Bulk Modulus

Here we derive Eq. (2.32). In a cubic material, $V = ca^3$ per atom, where

$$c = \begin{cases} \frac{1}{4} & \text{fcc} \\ \frac{1}{2} & \text{bcc} \\ 1 & \text{B2} \end{cases} . \tag{B.1}$$

Note that

$$\begin{aligned} \frac{\partial E}{\partial V} &= \frac{\partial E}{\partial a}\frac{\partial a}{\partial V} \\ \frac{\partial^2 E}{\partial V^2} &= \left(\frac{\partial a}{\partial V}\right)^2 \frac{\partial^2 E}{\partial a^2} + \frac{\partial E}{\partial a}\frac{\partial^2 a}{\partial V^2}. \end{aligned}$$

Thus, in B2 systems,

$$B = a^3\left[\frac{1}{(3a^2)^2}\frac{\partial^2 E}{\partial a^2} - \frac{2}{9a^5}\frac{\partial E}{\partial a}\right] = \frac{1}{9a}\frac{\partial^2 E}{\partial a^2} - \frac{2}{9a^2}\frac{\partial E}{\partial a}. \tag{B.2}$$

At the minimum of energy versus lattice constant, $\frac{\partial E}{\partial a}\big|_{a_0} = 0$, so

$$B(a_0) = \frac{1}{9a_0}\frac{\partial^2 E}{\partial a^2}\bigg|_{a_0}. \tag{B.3}$$

At a_{expt}, however, the second term in Eq. (B.2) does not vanish.

References

[1] K. Gschneidner, A. Russell, A. Pecharsky, J. Morris, Z. Zhang, T. Lograsso, D. Hsu, C. H. Chester Lo, Y. Ye, and A. Slager. A family of ductile intermetallic compounds. *Nature Materials*, 2(9):587–591, 2003.

[2] A. M. Russell. Ductility in intermetallic compounds. *Adv. Eng. Mater.*, 5(9):629–639, 2003.

[3] A. M. Russell, Z. Zhang, K. A. Gschneidner, T. A. Lograsso, A. O. Pecharsky, A. J. Slager, and D. C. Kesse. Mechanical properties of single crystal YCu and $(Tb_{0.88}Dy_{0.12})$Zn B2 intermetallic compounds. *Intermetallics*, 13(6):565–571, 2005.

[4] K. Gschneidner. Private communication.

[5] M Yamguchi and Y. Umakoshi. The deformation behaviour of intermetallic superlattice compounds. *Prog. Mater. Sci.*, 34:1–148, 1990.

[6] I. Baker. A review of the mechanical properties of B2 compounds. *Mater. Sci. Eng. A*, 192(1):1–13, 1995.

[7] W. A. Rachinger and A. H. Cottrell. Slip in crystals of the caesium chloride type. *Acta Metall.*, 4:109, 1956.

[8] A. Ball and R. E. Smallman. The operative slip system and general plasticity of NiAl—II. *Acta Metall.*, 14(11):1517–1526, 1966.

[9] D. I. Potter. Prediction of the operative slip system in CsCl type compounds using anisotropic elasticity theory. *Mater. Sci. Eng.*, 5(4):201–209, 1970.

[10] A. M. Russell, Z. Zhang, T. A. Lograsso, C. C. H. Lo, A. O. Pecharsky, J. R. Morris, Y. Ye, K. A. Gschneidner, and A. J. Slager. Mechanical properties of single crystal YAg. *Acta Mater.*, 52(13):4033–4040, 2004.

[11] G. H. Cao, D. Shechtman, D. M. Wu, A. T. Becker, L. S. Chumbley, T. A. Lograsso, A. M. Russell, and K. A. Gschneidner. Determination of slip systems and their relation to the high ductility and fracture toughness of the B2 DyCu intermetallic compound. *Acta Mater.*, 55(11):3765–3770, 2007.

[12] J. R. Morris, Y. Ye, Y. B. Lee, B. N. Harmon, and K. Gschneidner. Ab initio calculation of bulk and defect properties of ductile rare-earth intermetallic compounds. *Acta Mater.*, 52(16):4849–4857, 2004.

[13] Q. Chen and S. B. Biner. Stability of perfect dislocations in rare-earth intermetallic compounds: YCu, YAg and YZn. *Acta Mater.*, 53(11):3215–3223, 2005.

[14] J. R. Morris and Y. Y. Ye. Phase stability and predicted stacking faults in ductile B2 intermetallics. *Acta Mater.*

[15] J. B. Liu, D. D. Johnson, and A. V. Smirnov. Predicting yield-stress anomalies in $L1_2$ alloys: Ni_3Ge-Fe_3Ge pseudo-binaries. *Acta Mater.*, 53(13):3601–3612, 2005.

[16] V. Paidar, D. P. Pope, and M. Yamaguchi. Structural stability and deformation behavior of $L1_2$ ordered alloys. *Scripta Metall.*, 15(9):1029–1031, 1981.

[17] G. Saada and P. Veyssiere. The dissociation of a screw superdislocation in the $L1_2$ structure. *Phil. Mag. A*, 66(6):1081–1103, 1992.

[18] G. Saada and P. Veyssiere. The dissociation of a screw superdislocation in the B2 structure. *Phys. Stat. Sol. B*, 172(1):309–323, 1992.

[19] F. R. N. Nabarro. Mathematical theory of stationary dislocations. *Advances in Physics*, 1(3):269–394, 1952.

[20] T. H. Courtney. *Mechanical Behavior of Materials*. McGraw-Hill, Boston, MA, 2^{nd} edition, 2000.

[21] D. Hull and D. J. Bacon. *Introduction to Dislocations*. Butterworth-Heinemann, Woburn, MA, 4^{th} edition, 2001.

[22] J. D. Eshelby. Uniformly moving dislocations. *Proc. Phys. Soc. A*, 62(5):307–314, 1949.

[23] W. T. Read. *Dislocations in Crystals*. McGraw-Hill, 1953.

[24] J. P. Hirth and J. Lothe. *Theory of Dislocations*. Krieger, Malabar, FL, 1992.

[25] A. K. Head. The [111] dislocation in a cubic crystal. *Phys. Stat. Sol.*, 6:461, 1964.

[26] Y. Q. Sun. Stability of APB-dissociated $\langle 111 \rangle$ screw superdislocations in B2-ordered structures. *Acta Metall. Mater.*, 43(10):3775–3782, 1995.

[27] M. J. Mehl, B. M. Klein, and D. A. Papaconstantopolous. First principles calculations of elastic properties of metals. In J. H. Westbrook and R. L. Fleischer, editors, *Intermetallic Compounds: Principles and Practice*, chapter 9, pages 195–210. Wiley, London, 1995.

[28] G. Kresse and J. Hafner. Ab initio molecular dynamics for liquid metals. *Phys. Rev. B*, 47(1):558–561, 1993.

[29] G. Kresse and J. Furthmüller. Efficient iterative schemes for ab initio total-energy calculations using a plane-wave basis set. *Phys. Rev. B*, 54(16):11169–11186, 1996.

[30] G. Kresse and J. Furthmüller. Efficiency of ab-initio total energy calculations for metals and semiconductors using a plane-wave basis set. *Comput. Mater. Sci.*, 6:15–50, 1996.

[31] D. Vanderbilt. Soft self-consistent pseudopotentials in a generalized eigenvalue formalism. *Phys. Rev. B*, 41(11):7892–7895, 1990.

[32] G. Kresse and J. Hafner. Norm-conserving and ultrasoft pseudopotentials for first-row and transition elements. *J. Phys. Condens. Matter*, 6(40):8245–8257, 1994.

[33] J. P. Perdew and A. Zunger. Self-interaction correction to density-functional approximations for many-electron systems. *Phys. Rev. B*, 23(10):5048–5079, 1981.

[34] J. P. Perdew and Y. Wang. Accurate and simple analytic representation of the electron-gas correlation energy. *Phys. Rev. B*, 45(23):13244–13249, 1992.

[35] H. J. Monkhorst and J. D. Pack. Special points for Brillouin-zone integrations. *Phys. Rev. B*, 13(12):5188–5192, 1976.

[36] A. van de Walle and G. Ceder. Correcting overbinding in local-density-approximation calculations. *Phys. Rev. B*, 59(23):14992–15001, 1999.

[37] T. Hong and A. J. Freeman. Effect of antiphase boundaries on the electronic structure and bonding character of intermetallic systems: NiAl. *Phys. Rev. B*, 43(8):6446–6458, 1991.

[38] W. B. Pearson. *A Handbook of Lattice Spacings and Structures of Metals and Alloys*, volume 2. Pergamon, Oxford, 1967.

[39] D. Seipler, B. Bremicker, U. Goebel, H. Happel, H. E. Hoenig, and B. Perrin. Electronic structure of intermetallic compounds with CsCl structure. *J. Phys. F*, 7(4):599–611, 1977.

[40] D. G. Nagengast, A. T. M. van Gogh, E. S. Kooij, B. Dam, and R. Griessen. Contrast enhancement of rare-earth switchable mirrors through microscopic shutter effect. *Appl. Phys. Lett.*, 75(14):2050–2052, 1999.

[41] G. Simmons and H. Wong. *Single Crystal Elastic Constants and Calculated Aggregate Properties: A Handbook*. M.I.T. Press, Cambridge, MA, 2nd edition, 1971.

[42] R. J. Schiltz Jr., T. S. Prevender, and J. F. Smith. Single crystalline elastic constants of AuZn and YZn. *Journal of Applied Physics*, 42(12):4680–4684, 1971.

[43] D. Lazarus. The variation of the adiabatic elastic constants of KCl, NaCl, CuZn, Cu, and Al with pressure to 10,000 bars. *Phys. Rev.*, 76(4):545–553, 1949.

[44] S. Satpathy. Electron energy bands and cohesive properties of CsCl, CsBr, and CsI. *Phys. Rev. B*, 33(12):8706–8715, 1986.

[45] A. Smakula and J. Kalnajs. Precision determination of lattice constants with a Geiger-counter x-ray diffractometer. *Phys. Rev.*, 99(6):1737–1743, 1955.

[46] M. Yamaguchi and Y. Umakoshi. The operative slip systems and slip line morphology in βCuZn and β(CuNi)Zn alloys. *Acta Metall.*, 24(11):1061–1067, 1976.

[47] D. Wu, I. Baker, P. R. Munroe, and E. P. George. The yield strength anomaly of single-slip-oriented Fe–Al single crystals. *Intermetallics*, 15:103–107, 2007.

[48] T. Yamagata and H. Yoshida. Deformation behavior of FeAl single crystals. *Mater. Sci. Eng.*, 12(2):95–100, 1973.

[49] T. Yamagata. Correlation between characters of dislocations and operative slip systems in CsCl-type intermetallic compounds. *J. Phys. Soc. Jpn.*, 45(5):1575–1582, 1978.

[50] J. Brown, R. Srinivasan, M. J. Mills, and M. S. Daw. The mechanics of slip transition at intermediate temperatures in $\langle 001 \rangle$-oriented NiAl single crystals II. A metastable state for $a\langle 111 \rangle \{110\}$ dislocations in NiAl and its role in their decomposition. *Phil. Mag. A*, 80(12):2855–2870, 2000.

[51] C. L. Fu and M. H. Yoo. Deformation behavior of B2 type aluminides: FeAl and NiAl. *Acta Metall. Mater.*, 40(4):703–711, 1992.

[52] H. Saka, M. Kawase, A. Nohara, and T. Imura. Anti-phase boundary energy in β-CuZn. *Phil. Mag. A*, 50(1):65–70, 1984.

[53] G. Dirras, P. Beauchamp, and P. Veyssiere. Weak-beam study of the dislocation microstructure of β-CuZn deformed in the temperature domain of the plastic anomaly. *Phil. Mag. A*, 65(4):815–828, 1992.

[54] A. Smakula and M. W. Klein. Investigation of the gliding process in ionic crystals by prismatic punching. *Phys. Rev.*, 84(5):1043–1049, 1951.

Vita

Ruoshi Sun was born in Beijing in 1986. At the age of 5, he went to the US with his parents, where he attended Martin Luther King, Jr. Elementary School in Urbana, IL until he was $7\frac{1}{2}$ years old. After moving to Hong Kong, he studied at Kiangsu and Chekiang Primary School from second grade to sixth grade, and St. Paul's Co-educational College from Form 1 to Form 6. He came to the US again in 2004 for college education. Having been accepted to the Ph.D. program in Materials Science and Engineering at MIT, he will continue his studies there for the next few years.

Education

B.S. Materials Science and Engineering, Mathematics, University of Illinois at Urbana-Champaign, 2008

Research Experience

REU Program, UIUC, Summer 2007

Ab initio density-functional calculations of defect energies in CoPt and FePd

Advisor: Prof. Duane D. Johnson

REU Program, UIUC, Summer 2006

Molecular dynamics and electron diffraction simulation of Au nanoparticles

Advisor: Prof. Jian-Min Zuo

Publications

1. Ruoshi Sun and D. D. Johnson, "First-principles design maps for predicting anomalous ductility in B2 materials," in preparation.

2. J. B. Liu, B. Kraczek, Ruoshi Sun, and D. D. Johnson, "Structural defect energies in magnetic Co-Pt-type compounds: Effect of processing temperatures," in preparation.

3. W. J. Huang, R. Sun, J. Tao, L. D. Menard, R. G. Nuzzo, and J. M. Zuo, "Coordination dependent surface atomic contraction in nanocrystals revealed by coherent diffraction," *Nature Materials* **7**, 308–313 (2008). (doi:10.1038/nmat2132)

4. W. J. Huang, B. Jiang, R. S. Sun, and J. M. Zuo, "Towards sub-Å atomic resolution electron diffraction imaging of metallic nanoclusters: A simulation study of experimental parameters and reconstruction algorithms," *Ultramicroscopy* **107**, 1159–1170 (2007). (doi:10.1016/j.ultramic.2007.01.017)

Conferences and Symposiums

1. Ruoshi Sun and Duane D. Johnson, "First-principles design maps for predicting anomalous ductility in B2 materials," Undergraduate Research Symposium, UIUC, 2008.

2. Weijie Huang, Ruoshi Sun, Laurent Menard, Ralph Nuzzo, and Jian-Min Zuo, "Surface atomic contraction in nanocrystals revealed by coherent diffraction," MRS Fall Meeting, Boston, MA, 2007.

Honors and Awards

1. Bronze Tablet (top 3% of graduating class), 2008

2. Most Outstanding Undergraduate Major Award in Mathematics, 2008

3. James Scholar, 2004 – 08
4. Dean's List, 2004 – 08
5. Clifton G. Bergeron Scholarship, 2007 – 08
6. Sam & Dubey Portnoy Scholarship, 2007 – 08
7. Caterpillar Scholar, 2006 – 07
8. Kimberly-Clark Scholar, 2005 – 06
9. Alfred W. Allen Award, 2005
10. Mothers Association Book Award, 2005
11. Racheff Ivan Undergraduate Award, 2004 – 05

Computer Skills

C, UNIX, LaTeX, MATLAB, Mathematica, DigitalMicrograph, AutoCAD

Language Skills

Fluent in English, native speaker of Chinese (Mandarin and Cantonese)

Extracurricular Activities

Group leader of Engineering Open House project on nanotechnology: Exhibited at the Museum of Science and Industry in Chicago, March 2005

Members: Illini Chinese Christian Fellowship, Undergraduate Materials Organization

Hobbies: Piano, weiqi/go, ping-pong